Discrete-time analysis of Schwarz waveform relaxation convergence

Arthur Arnoult, Caroline Japhet, Pascal Omnes

DISCRETE-TIME ANALYSIS OF OPTIMIZED SCHWARZ WAVEFORM RELAXATION CONVERGENCE

ARTHUR ARNOULT[‡], CAROLINE JAPHET[‡] AND PASCAL OMNES[§‡]

Abstract. We propose a new approach to analyze the convergence of optimized Schwarz waveform relaxation (OSWR) iterations for parabolic problems. Departing from traditional Fourier analysis in the time direction, we explicitly solve the equations obtained using the backward Euler scheme in time, and deduce convergence properties from this solution, in the two subdomains case. Convergence is proven for any positive Robin parameter (or couple of such parameters in the two-sided case). We also show that, for any fixed value of the number of time steps, the convergence depends on a single parameter which is a combination of the diffusion coefficient, the time step and the Robin parameter. A convergence result in a finite number of iterations is also proven for a well-chosen value of the Robin parameters. This approach allows us to define efficient optimized Robin parameters that depend on the number of iterations one wishes to perform, and to recommend a couple (number of iterations, Robin parameter) to reach a given accuracy. Numerical experiments illustrate the performance of such iteration-dependent optimized Robin parameters, compared to the observed optimal ones (which also depend on the number of iterations performed). A comparison is also given with optimized parameters derived by classical Fourier transform analysis on the continuous problem (which are independent of the iterations).

Key words. Optimized Schwarz waveform relaxation, Robin transmission conditions, Discrete-time convergence analysis, Iteration-dependent Robin parameters.

1. Introduction.

Schwarz Waveform Relaxation (SWR) algorithms [11, 18, 19], and their extensions, have a long history in the parallel solution of discretized time-dependent models driven by partial differential equations, such as those arising in engineering, physics, porous media or geophysical applications, etc [15, 33, 9, 22, 3, 26, 7, 5, 38, 1, 36]. The success of these iterative methods is linked to their fast convergence that can be optimized by choosing appropriate boundary conditions on the space-time interfaces between subdomains. In this contribution, we consider Robin boundary conditions without overlap, in which the value of the Robin parameter(s) can be chosen identically on the two sides of the interface (the so-called one-sided case), or differently (the two-sided case), and can be optimized to improve convergence rates. The corresponding algorithm is called Optimized Schwarz Waveform Relaxation (OSWR), see [15, 32, 14]. These methods are well-suited to handle nonconformities in time and space, and can be combined with a posteriori estimates (to get efficient stopping criteria) or time parallelization techniques [23, 2, 21, 16, 6].

Traditional convergence analysis of OSWR algorithms is mostly performed using the continuous model, in an attempt to obtain a theory which is independent of the actual numerical schemes used for discretization. This analysis may be performed by energy estimates, both in the one-sided and two-sided cases [23, 25]. This technique is quite general but does not provide a convergence rate, nor a hint on how to properly choose the Robin parameters for fast convergence. At the discrete-time level, a convergence proof by energy estimates is performed for the one-sided case [23], but not for the two-sided case.

On the other hand, Fourier transforms in time and space are commonly used at the continuous level to obtain convergence rates of the OSWR method for each Fourier mode [27, 12, 15, 32, 14]; although the supremum of this convergence factor

[‡]CNRS, UMR 7539, Laboratoire de Géométrie, Analyse et Applications, LAGA, Université Sorbonne Paris Nord, F-93430, Villetaneuse, France,
(arnoult@math.univ-paris13.fr, japhet@math.univ-paris13.fr).
[§]CEA Saclay, DM2S-STMF, F-91191 Gif sur Yvette Cedex, France (pascal.omnes@cea.fr).

over the whole Fourier space is one, it can however be used to choose efficient Robin parameters that optimize it over the bounded range of frequencies relevant to the discrete numerical (time and space) grids. However, actual numerical results obtained with this choice of Robin parameters do not always perform as efficiently as expected and it has been discussed that the Fourier transform in time may not always allow to perform an adequate analysis of the convergence properties of the method [35, 17]. This may be due to the fact that the Fourier transform supposes an infinite time interval, while the actual simulation is necessarily performed on a finite one; switching to Fourier series does not solve this issue since the error does not vanish at the final time as it does at the initial time. Another approach, based on discrete-time analysis is proposed in [8, 24]; for simple schemes, it is based on the so-called one-sided $\mathcal{Z}$ transform, which is a discrete equivalent of the Laplace transform. However, this also requires either to consider infinite intervals in time or to neglect the error at the final time. On the contrary, in the present contribution we do not perform any transformation in the time direction; restricting for the sake of simplicity to the one-dimensional heat equation in the two subdomains case, we solve directly the full space-time semi-discrete system on any finite time interval; this is made possible by the Jordan form of the backward Euler scheme that is used to discretize in the time direction.

This approach is particularly rich and allows to obtain several new results: first, we prove convergence of the discrete-time one-sided and two-sided algorithms for any positive value of the Robin coefficients, with a convergence that, for any fixed value of the number of time steps, depends on a single parameter in the one-sided case (and on two parameters in the two-sided case) which is a combination of the diffusion coefficient value, the time step and the Robin parameter; secondly, we obtain exact convergence of the OSWR for a well-chosen value of the Robin parameters in a number of iterations equal to the number of time steps (one-sided case) or twice this number (two-sided case). Furthermore, numerical simulations show that the observed optimal Robin parameter depends itself on the number of iterations performed, and we propose a method to choose an efficient parameter as a function of this number; this allows us to recommend a couple (number of iterations, Robin parameter) to reach a given accuracy, e.g. the expected scheme accuracy.

This paper is organized as follows: in Section 2, we consider a model problem and state its well-posedness, as well as that of the equivalent multi-domain problem. Then we introduce the discrete-time multi-domain problem, using an implicit Euler scheme. This problem involves a matrix on which our analysis depends; some of its properties are given in Section 3. In Section 4, we first recall the continuous OSWR method, and the usual approach to calculate optimized Robin parameters using Fourier transform in time. Then we consider the discrete-time OSWR algorithm and prove its convergence, as well as various related properties. The main result of this article is an estimate of the relative convergence error at each iteration, which allows to introduce a new strategy to define discrete-time optimized parameters that depend on the number of iterations that will be performed. Finally, in Section 5, numerical experiments show that the proposed error estimate is close to the relative convergence error at each iteration. Numerical results comparing convergence with continuous or discrete-time optimized Robin parameters show that, even if the continuous ones can be a reasonable choice in some cases, the discrete-time ones give better performances, as they are close to the iteration dependent numerical optimal ones, in all test cases. Asymptotic performance with these optimized parameters shows that the convergence depends weakly (one-sided) and is almost independent (two-sided) of the time step.

2. Problem Setting. In order to simplify the analysis, we consider the following monodimensional heat equation on $\Omega \times (0,T)$, with $\Omega = \mathbb{R}$ and $T > 0$ the final time,

$$\begin{array}{rll} \mathcal{L}u \coloneqq \partial_t u - \nu \partial_{xx} u &= f & \text{in } \Omega \times (0,T), \\ u(\cdot\,, t=0) &= u_0 & \text{in } \Omega, \\ \lim\limits_{x \to \pm\infty} u(x,\cdot) & & \text{is bounded,} \end{array} \tag{2.1}$$

where f is a source term, u_0 an initial condition and ν a positive diffusion coefficient.

Let $H^{r,s}(\Omega \times (0,T)) = L^2(0,T;H^r(\Omega)) \cap H^s(0,T;L^2(\Omega))$ be anisotropic Sobolev spaces defined in [29]. Let us recall Propositions 2.1 and 2.2 below, that can be directly deduced from [30].

PROPOSITION 2.1. *If u_0 belongs to $H^1(\Omega)$ and f to $L^2(0,T;L^2(\Omega))$, then problem (2.1) admits a unique solution in $H^{2,1}(\Omega \times (0,T))$.*

Let us consider a decomposition of Ω into two non-overlapping subdomains

$$\Omega_1 = (-\infty, 0), \quad \Omega_2 = (0, +\infty),$$

and introduce the Robin interface operators as follows (see [31, 14])

$$\mathcal{B}_1 = \nu \partial_x + \alpha_1, \qquad \mathcal{B}_2 = -\nu \partial_x + \alpha_2. \tag{2.2}$$

Then, problem (2.1) can be reformulated as the following equivalent multi-domain problem, with $f_i = f_{|\Omega_i}$, $u_i = u_{|\Omega_i}$, and $u_{0,i} = u_{0|\Omega_i}$, $i = 1, 2$:

$$\begin{array}{rll} \mathcal{L}u_1 &= f_1 & \text{in } \Omega_1 \times (0,T), \\ \mathcal{B}_1 u_1 &= \mathcal{B}_1 u_2 & \text{on } \{0\} \times (0,T), \\ u_1(\cdot,0) &= u_{0,1} & \text{in } \Omega_1, \\ \lim\limits_{x \to -\infty} u_1(x,\cdot) & & \text{is bounded,} \end{array} \qquad \begin{array}{rll} \mathcal{L}u_2 &= f_2 & \text{in } \Omega_2 \times (0,T), \\ \mathcal{B}_2 u_2 &= \mathcal{B}_2 u_1 & \text{on } \{0\} \times (0,T), \\ u_2(\cdot,0) &= u_{0,2} & \text{in } \Omega_2, \\ \lim\limits_{x \to +\infty} u_2(x,\cdot) & & \text{is bounded.} \end{array} \tag{2.3}$$

The Robin parameters α_1, α_2 involved in (2.3) (through $\mathcal{B}_i$, $i = 1, 2$, defined in (2.2)) are freely chosen positive real numbers chosen such that : a) the Robin subdomain problems in (2.3) are well posed (see e.g. [30, 6]), b) they lead to a fast converging OSWR algorithm (see Section 4).

PROPOSITION 2.2. *Let $i = 1$ or $i = 2$. If $u_{0,i} \in H^1(\Omega_i)$, $f_i \in L^2(0,T;L^2(\Omega_i))$, and $\mathcal{B}_i u_j \in H^{\frac{1}{4}}(0,T)$, with $j = 3 - i$, then the Robin subdomain problem in Ω_i in (2.3) has a unique solution in $H^{2,1}(\Omega_i \times (0,T))$.*

In practice, a problem such as (2.3) is solved approximately through discretization and approximation of the derivatives of u by discrete formulas. In this article, we are concerned with the implicit Euler approximation of the time derivative (with uniform time step Δt). Thus, we consider the following semi-discrete approximation of (2.3): Find $U_i = (U_{i,1} \dots U_{i,N})^T$, for $i = 1, 2$, such that

$$\begin{array}{rll} LU_1 &= F_1 & \text{in } \Omega_1, \\ B_1 U_1 &= B_1 U_2 & \text{at } x = 0, \\ \lim\limits_{x \to -\infty} U_1(x) & & \text{is bounded,} \end{array} \qquad \begin{array}{rll} LU_2 &= F_2 & \text{in } \Omega_2, \\ B_2 U_2 &= B_2 U_1 & \text{at } x = 0, \\ \lim\limits_{x \to +\infty} U_2(x) & & \text{is bounded,} \end{array} \tag{2.4}$$

with operator $L : \mathbb{R}^N \to \mathbb{R}^N$ defined as follows

$$LU_i \coloneqq \frac{1}{\nu \Delta t} A U_i - U_i'', \qquad i = 1, 2,$$

where $A \in \mathbb{R}^{N \times N}$ is defined by

$$A \coloneqq \begin{pmatrix} 1 & & & \\ -1 & 1 & & \\ & \ddots & \ddots & \\ & & -1 & 1 \end{pmatrix}, \tag{2.5}$$

and where, for $i = 1, 2$, for all $n \in [\![1, N]\!]$, $U_{i,n}(x)$ is an approximation of $u_i(x, n\Delta t)$, and $F_i = (F_{i,1} \dots F_{i,N})^T$, with $F_{i,n}(x) \coloneqq \frac{f_i(x, n\Delta t)}{\nu} + \frac{u_0(x)}{\nu \Delta t} \delta_{1n}$ (where δ_{1n} is the Kronecker delta). The discrete interface operators B_1 and B_2 are extensions of $\mathcal{B}_1$ and $\mathcal{B}_2$ to vectors in $\mathbb{R}^N$.

The analysis performed in this article relies on various properties of matrix A, which are presented in the next section.

3. Jordan decomposition.

As we will see in Section 3.3, solving (2.4) will involve a square root of matrix A. Therefore, we will prove that it exists, using the Jordan decomposition of A. This decomposition will also be very useful for the analysis of the OSWR algorithm in Section 4.

3.1. Definitions and general results.

We recall here some definitions and results about matrix exponential, square root of a matrix and Jordan decomposition, from [34, 37, 20].

Definition 3.1 (Square root of a matrix). *A square root of a matrix M is a matrix whose square is M. It might not exist nor be unique.*

Definition 3.2 (Matrix exponential). *If M is a square matrix, the exponential of M is the matrix defined by*

$$\exp(M) = \sum_{k=0}^{+\infty} \frac{M^k}{k!}.$$

We recall the following property about matrix exponential from [34, Page 79].

Proposition 3.3. *The function $\varphi : x \in \mathbb{C} \mapsto \exp(xM)$, where M is a square matrix, is differentiable with respect to x and $\frac{\partial \varphi}{\partial x}(x) = M \exp(xM) = \exp(xM)\, M$.*

We recall the following results (Definition 3.4 and Theorem 3.5) about Jordan decomposition from [37, Page 350] and [20, Page 317].

Definition 3.4 (Jordan block). *The Jordan block of parameter μ and size r_k is the $r_k \times r_k$ matrix ($r_k \in \mathbb{N}^*$), defined by*

$$J_\mu = \begin{pmatrix} \mu & 1 & & 0 \\ & \ddots & \ddots & \\ & & \ddots & 1 \\ 0 & & & \mu \end{pmatrix}.$$

THEOREM 3.5 (Jordan decomposition). *If $M \in \mathbb{C}^{N\times N}$, then there exists a non-singular matrix $X \in \mathbb{C}^{N\times N}$ such that*

$$XMX^{-1} = \begin{pmatrix} J_{\mu_1} & & 0 \\ & \ddots & \\ 0 & & J_{\mu_K} \end{pmatrix},$$

where $\mu_1, \dots \mu_K$ are the eigenvalues of M, possibly equal. The number of Jordan blocks associated with an eigenvalue is equal to its geometric multiplicity, i.e. the dimension of the associated eigenspace.

PROPOSITION 3.6 (Commuting two Jordan blocks of same size). *Blocks J_λ and J_μ commute (and thus also J_λ^{-1} and J_μ^{-1}), as well as J_λ^{-1} and J_μ.*

3.2. Square root of a matrix. In this part, we prove that a Jordan matrix admits a square root.

PROPOSITION 3.7. *Every matrix $M = \mu \boldsymbol{I}_N + \mathcal{N}$ with μ nonzero and $\mathcal{N}$ a nilpotent matrix admits a square root under the form*

$$\sqrt{M} \coloneqq \sqrt{\mu} \sum_{k=0}^{N} \binom{\frac{1}{2}}{k} \frac{1}{\mu^k} \mathcal{N}^k, \tag{3.1}$$

with generalized binomial coefficients :

$$\binom{\frac{1}{2}}{0} \coloneqq 1, \qquad \binom{\frac{1}{2}}{k} \coloneqq \frac{\frac{1}{2}(\frac{1}{2}-1)\dots(\frac{1}{2}-k+1)}{k!}, \ \forall k \geq 1.$$

Proof. Let us start with the case where $\mu = 1$. Let d be the index of $\mathcal{N}$. If $d = 1$ then $\mathcal{N} = 0_{N,N}$, thus $M = \mathbf{I}_N$, and (3.1) gives $\sqrt{M} = \mathbf{I}_N$, which is indeed a square root of M. If $d > 1$, let

$$P_{d-1}(X) = \sum_{k=0}^{d-1} \binom{\frac{1}{2}}{k} X^k.$$

We will prove that $P_{d-1}^2(\mathcal{N}) = \mathbf{I}_N + \mathcal{N}$, i.e. that the polynomial R defined by $R(X) \coloneqq 1 + X - P_{d-1}^2(X)$ vanishes in matrix $\mathcal{N}$. For this, we will first show that R is factorizable as a product of X^d and a polynomial, and then use that $\mathcal{N}^d = 0$.

The polynomial P_{d-1} has been chosen as the $(d-1)$-order Taylor expansion of $t \mapsto \sqrt{1+t}$ around 0 :

$$\sqrt{1+t} \underset{t\to 0}{=} P_{d-1}(t) + o(t^{d-1}).$$

By squaring the above equality, we get

$$1 + t = \sqrt{1+t}^2 \underset{t\to 0}{=} P_{d-1}^2(t) + 2P_{d-1}(t)o(t^{d-1}) + o(t^{d-1})^2 = P_{d-1}^2(t) + o(t^{d-1}). \tag{3.2}$$

The polynomial R being of degree $2d-2$, it can be written under the form $R(X) = \sum_{k=0}^{2d-2} \eta_k X^k$, with $\eta_k \in \mathbb{R}$ and $\eta_{2d-2} \neq 0$. Then, from (3.2) and the definition of R, one gets $R(t) \underset{t\to 0}{=} o(t^{d-1})$ which is only possible if all η_k are zeros for $k \in [\![0, d-1]\!]$. This implies that

$$R(X) = \sum_{k=d}^{2d-2} \eta_k X^k = \sum_{k=0}^{d-2} \eta_{k+d} X^{k+d} = X^d \sum_{k=0}^{d-2} \eta_{k+d} X^k.$$

Using that $\mathcal{N}$ is a nilpotent matrix of index d, i.e. $\mathcal{N}^d = 0$, if follows that $R(\mathcal{N}) = 0$. According to the definition of R, we obtain :

$$\mathbf{I}_N + \mathcal{N} = P_{d-1}^2(\mathcal{N}).$$

Let us now consider the general case, with μ nonzero, arbitrary. We can rewrite M as $M = \mu(\mathbf{I}_N + \frac{1}{\mu}\mathcal{N})$ where the $\frac{1}{\mu}\mathcal{N}$ is nilpotent of index d, and then apply the above result to define $\sqrt{M}$ by

$$\sqrt{M} \coloneqq \sqrt{\mu}\, P_{d-1}\left(\frac{1}{\mu}\mathcal{N}\right),$$

with $\sqrt{\mu}$ a complex number whose square is μ. ∎

COROLLARY 3.8. *If μ is nonzero, J_μ admits a square root. In this case, $\mathcal{N}$ is the matrix with 1 on the superdiagonal, and 0 elsewhere. Then the i-th superdiagonal of $\sqrt{J_\mu}$ only contains coefficient $\mu^{\frac{1}{2}-i}\binom{\frac{1}{2}}{i}$.*

3.3. Application to matrix A. Let us now prove that matrix A (defined in (2.5)) admits a square root and give the Jordan decomposition of the latter. The following proposition is immediate.

PROPOSITION 3.9 (Eigenvalue and eigenspace of A). *The only eigenvalue of A is 1 and the associated eigenspace is of dimension one:*

$$S_1(A) = \mathrm{Span}\big((0,\dots,0,1)^{\mathrm{T}}\big). \tag{3.3}$$

PROPOSITION 3.10 (Definition and properties of $\sqrt{A}$). *Matrix A admits a square root with the following properties :*

(i) The only eigenvalue of $\sqrt{A}$ is 1 and the associated eigenspace is $S_1(A)$ defined in (3.3).

(ii) $\sqrt{A}$ admits a Jordan decomposition

$$\sqrt{A} = Q^{-1}J_1Q, \tag{3.4}$$

with Q an invertible matrix and J_1 as in Definition 3.4 with $\mu = 1$.

Proof. Since $A = \mathbf{I}_N + \mathcal{N}$, where $\mathcal{N}$ is the strictly lower triangular matrix with coefficient -1 on the first lower diagonal, Proposition 3.7 shows that A admits a square root given by formula (3.1), which additionally shows that 1 is the only eigenvalue of $\sqrt{A}$, since all powers of $\mathcal{N}$ are also strictly lower triangular.

Furthermore, let X be a nonzero eigenvector associated with the eigenvalue of $\sqrt{A}$. We thus have: $\sqrt{A}X = X$. Then $AX = \sqrt{A}\sqrt{A}X = \sqrt{A}X = X$. As X is nonzero, it is also an eigenvector of A, and, according to Proposition 3.9, X is necessarily collinear to $(0,\dots,0,1)^T$. This shows (i).

From (i) and Theorem 3.5, we obtain the Jordan decomposition (ii). ∎

4. OSWR algorithm. In this section, after recalling some results in the continuous framework, we study the convergence of the discrete-time OSWR algorithm. This will then suggest a methodology for calculating the Robin parameters.

4.1. Continuous case. The OSWR method for solving (2.3) consists in choosing initial Robin data ξ_1^0, ξ_2^0 on $(0,T)$, and setting $\mathcal{B}_1 u_2^0(0,\cdot) \coloneqq \xi_1^0$, $\mathcal{B}_2 u_1^0(0,\cdot) \coloneqq \xi_2^0$.

Then for $\ell = 1, 2, \ldots$ one solves the local Robin problems

$$\begin{array}{rll} \mathcal{L}u_1^\ell &= f_1 & \text{in } \Omega_1 \times (0,T), \\ \mathcal{B}_1 u_1^\ell &= \mathcal{B}_1 u_2^{\ell-1} & \text{on } \{0\} \times (0,T), \\ u_1^\ell(\cdot,0) &= u_{0,1} & \text{in } \Omega_1, \\ \lim\limits_{x\to-\infty} u_1^\ell(x,\cdot) & & \text{is bounded,} \end{array} \qquad \begin{array}{rll} \mathcal{L}u_2^\ell &= f_2 & \text{in } \Omega_2 \times (0,T), \\ \mathcal{B}_2 u_2^\ell &= \mathcal{B}_2 u_1^{\ell-1} & \text{on } \{0\} \times (0,T), \\ u_2^\ell(\cdot,0) &= u_{0,2} & \text{in } \Omega_2, \\ \lim\limits_{x\to+\infty} u_2^\ell(x,\cdot) & & \text{is bounded.} \end{array}$$

The usual Fourier transform in time approach (with the assumption of an infinite time interval) provides an expression of the convergence factor of the above algorithm (see [13, 14]) as follows

$$\rho(\omega, \alpha_1, \alpha_2) \coloneqq \left(\frac{\sqrt{i\omega} - \alpha_1}{\sqrt{i\omega} + \alpha_1}\right)\left(\frac{\sqrt{i\omega} - \alpha_2}{\sqrt{i\omega} + \alpha_2}\right),$$

for all Fourier time frequencies ω. While we have $\max\limits_{\omega\in\mathbb{R}} |\rho(\omega, \alpha_1, \alpha_2)| = 1$, the convergence factor can be used to calculate efficient Robin parameters in the discrete setting. Indeed, in numerical computations the time frequency is bounded, i.e. in $[\frac{\pi}{T}, \frac{\pi}{\Delta t}]$. Then, one can define *continuous optimized Robin parameters* $\alpha_{1,C}$, $\alpha_{2,C}$ such that

$$|\rho(\omega, \alpha_{1,C}, \alpha_{2,C})| = \min_{(\alpha_1,\alpha_2)\in(\mathbb{R}^{+*})^2} \max_{\omega\in[\frac{\pi}{T},\frac{\pi}{\Delta t}]} |\rho(\omega, \alpha_1, \alpha_2)|,$$

see e.g. [28, 32, 12, 14]. One can also consider the one-sided case $\alpha \coloneqq \alpha_1 = \alpha_2$ and define α_C as the solution of the above minimization problem on $\alpha \in \mathbb{R}^{+*}$. In our numerical experiments of Section 5, the minimization is done using the GNU Octave *fminsearch* function [10].

4.2. Dimensionless Robin parameters. In what follows, we will use the notation below, for dimensionless Robin parameters:

$$\bar{\alpha}_i \coloneqq \alpha_i \sqrt{\frac{\Delta t}{\nu}}, \quad i = 1, 2, \qquad \bar{\boldsymbol{\alpha}} \coloneqq (\bar{\alpha}_1, \bar{\alpha}_2). \tag{4.1}$$

This notation will be useful for the convergence analysis in the discrete-time setting. More precisely, we will observe in Section 4.4 that the convergence depends only on $\bar{\boldsymbol{\alpha}}$ and N.

Using this notation, the *dimensionless continuous optimized Robin parameters,* for the one and two-sided cases, are respectively denoted by

$$\bar{\alpha}_C \coloneqq \alpha_C \sqrt{\frac{\Delta t}{\nu}}, \qquad \bar{\boldsymbol{\alpha}}_C \coloneqq \sqrt{\frac{\Delta t}{\nu}}(\alpha_{1,C}, \alpha_{2,C}). \tag{4.2}$$

4.3. Discrete-time algorithm. The discrete-time OSWR algorithm for solving the coupled problem (2.4) is as follows.

Algorithm 4.1 (Discrete-time OSWR)

Choose initial Robin data $\Xi_1^0, \Xi_2^0 \in \mathbb{R}^N$ at $x = 0$, and set $B_1U_2^0 := \Xi_1^0$, $B_2U_1^0 := \Xi_2^0$
for $\ell = 1, 2, \dots$ **do**
Solve the local Robin problems

$$\begin{array}{llll} LU_1^\ell & = F_1 & \text{in } \Omega_1, & \\ B_1U_1^\ell & = B_1U_2^{\ell-1} & \text{at } x = 0, & \\ \lim\limits_{x\to-\infty} & U_1^\ell(x) & \text{is bounded,} & \end{array} \qquad \begin{array}{llll} LU_2^\ell & = F_2 & \text{in } \Omega_2, & \\ B_2U_2^\ell & = B_2U_1^{\ell-1} & \text{at } x = 0, & \\ \lim\limits_{x\to+\infty} & U_2^\ell(x) & \text{is bounded.} & \end{array} \tag{4.3}$$

end for

In what follows, an analysis of the convergence of Algorithm 4.1 is given.

4.4. Discrete-time convergence analysis. Let us denote by (U_1, U_2) the solution of (2.4). Then, by linearity, the error $E_i^\ell = U_i^\ell - U_i,\ i = 1, 2$, at iteration ℓ of Algorithm 4.1, satisfy (4.3) with $F_i = 0_N,\ i = 1, 2$.

For $\ell \geq 1$ fixed, let us first consider the subdomain problems without the Robin transmission conditions :

$$\begin{array}{llll} LE_1^\ell & = 0_N & \text{in } \Omega_1, & \\ \lim\limits_{x\to-\infty} & E_1^\ell(x) & \text{is bounded.} & \end{array} \qquad \begin{array}{llll} LE_2^\ell & = 0_N & \text{in } \Omega_2, & \\ \lim\limits_{x\to+\infty} & E_2^\ell(x) & \text{is bounded.} & \end{array} \tag{4.4}$$

Then we have the following result:

THEOREM 4.1. *Let $\ell \geq 1$. There exists $\beta_i^\ell \in \mathbb{R}^N,\ i = 1, 2$, such that the subdomain solutions of (4.4) are of the form*

$$E_i^\ell(x) = \mathrm{e}^{\frac{-|x|}{\sqrt{\nu\Delta t}}\sqrt{A}}\beta_i^\ell \qquad \forall x \in \Omega_i, \quad i = 1, 2. \tag{4.5}$$

The proof of Theorem 4.1 is given in Appendix 6.1.

Let us introduce the dimensionless initial Robin data for the errors

$$\bar{G}_i^0 := \sqrt{\frac{\Delta t}{\nu}}\big(\Xi_i^0 - (B_iU_i)(0)\big), \quad i = 1, 2. \tag{4.6}$$

Let us also extend (4.5) to the case $\ell = 0$, for $\bar{\alpha}_j \neq 1,\ j = 1, 2$,

$$\beta_i^0 := \left(\bar{\alpha}_j\mathbf{I}_N - \sqrt{A}\right)^{-1}\bar{G}_j^0, \quad j = 3 - i, \quad i = 1, 2, \tag{4.7}$$

$$E_i^0(x) := \mathrm{e}^{\frac{-|x|}{\sqrt{\nu\Delta t}}\sqrt{A}}\beta_i^0, \qquad \forall x \in \Omega_i, \quad i = 1, 2. \tag{4.8}$$

For $\ell \geq 1$, the dimensionless Robin data for the errors are denoted by

$$\bar{G}_i^\ell := \sqrt{\frac{\Delta t}{\nu}}(B_i(E_j^\ell))(0) = \left(\bar{\alpha}_i\mathbf{I}_N - \sqrt{A}\right)\beta_j^\ell, \qquad j = 3 - i,\ i = 1, 2. \tag{4.9}$$

Let $\boldsymbol{H}^1(\Omega_i) := (H^1(\Omega_i))^N$ and $\boldsymbol{L}^\infty(\Omega_i) := (L^\infty(\Omega_i))^N$, equipped respectively with

$$\|U\|_{\boldsymbol{H}^1(\Omega_i)} := \sqrt{\sum_{j\in[\![1,N]\!]}(\|U_j\|^2_{H^1(\Omega_i)})}, \quad \|U\|_{\boldsymbol{L}^\infty(\Omega_i)} := \max_{j\in[\![1,N]\!]}(\|U_j\|_{L^\infty(\Omega_i)}).$$

With these notations and Theorem 4.1, we can now prove the convergence of Algorithm 4.1.

THEOREM 4.2 (OSWR convergence). *Let $\alpha_i > 0,\ i = 1, 2$. Then, Algorithm 4.1 converges in $\left(\boldsymbol{H}^1(\Omega_1) \cap \boldsymbol{L}^\infty(\Omega_1)\right) \times \left(\boldsymbol{H}^1(\Omega_2) \cap \boldsymbol{L}^\infty(\Omega_2)\right)$ to the solution of (2.4). Moreover, setting*[*]

$$M(\bar{\boldsymbol{\alpha}}) := \left(\bar{\alpha}_i \boldsymbol{I}_N + \sqrt{A}\right)^{-1} \left(\bar{\alpha}_i \boldsymbol{I}_N - \sqrt{A}\right) \left(\bar{\alpha}_j \boldsymbol{I}_N + \sqrt{A}\right)^{-1} \left(\bar{\alpha}_j \boldsymbol{I}_N - \sqrt{A}\right), \quad (4.10)$$

we have the following relations on the Robin data for the errors, for i=1,2,

$$\bar{G}_i^{2\ell} = (M(\bar{\boldsymbol{\alpha}}))^\ell \bar{G}_i^0, \quad \forall \ell \geq 0, \quad (4.11a)$$

$$\bar{G}_i^{2\ell+1} = (M(\bar{\boldsymbol{\alpha}}))^\ell \bar{G}_i^1, \quad \forall \ell \geq 0, \quad (4.11b)$$

as well as the discrete-time relations for the errors on the interface[**]

$$\beta_i^{2\ell} = (M(\bar{\boldsymbol{\alpha}}))^\ell \beta_i^0 \quad \forall \ell \geq 0, \quad (4.12a)$$

$$\beta_i^{2\ell+1} = (M(\bar{\boldsymbol{\alpha}}))^\ell \beta_i^1 \quad \forall \ell \geq 0, \quad (4.12b)$$

from which we deduce the following convergence estimates, for even and odd iterations

$$\frac{\|E_i^{2\ell}(0)\|_\infty}{\|E_i^0(0)\|_\infty} \leq \|(M(\bar{\boldsymbol{\alpha}}))^\ell\|_\infty, \quad \forall \ell \geq 0, \quad (4.13a)$$

$$\frac{\|E_i^{2\ell+1}(0)\|_\infty}{\|E_i^1(0)\|_\infty} \leq \|(M(\bar{\boldsymbol{\alpha}}))^\ell\|_\infty, \quad \forall \ell \geq 0. \quad (4.13b)$$

Thus, $\|(M(\bar{\boldsymbol{\alpha}}))^\ell\|_\infty$ is an estimate of the relative L^∞-error at iterations 2ℓ and $2\ell+1$, for all $\ell \geq 0$.

Proof. Let us first prove (4.11) for $\ell \geq 1$ (the case $\ell = 0$ being trivial).

Replacing (4.5) in the Robin transmission conditions at $x = 0$ in (4.3), and using Proposition 3.3, lead to, for $i = 1, 2$,

$$\left(\alpha_i \mathbf{I}_N + \nu \frac{\sqrt{A}}{\sqrt{\nu \Delta t}}\right) \beta_i^1 = \Xi_i^0 - (B_i U_i)(0),$$

$$\left(\alpha_i \mathbf{I}_N + \nu \frac{\sqrt{A}}{\sqrt{\nu \Delta t}}\right) \beta_i^\ell = \left(\alpha_i \mathbf{I}_N - \nu \frac{\sqrt{A}}{\sqrt{\nu \Delta t}}\right) \beta_j^{\ell-1}, \quad j = 3 - i, \quad \forall \ell \geq 2,$$

or equivalently, using the dimensionless notations (4.1) and (4.6), for $i = 1, 2$,

$$\left(\bar{\alpha}_i \mathbf{I}_N + \sqrt{A}\right) \beta_i^1 = \bar{G}_i^0, \quad (4.14a)$$

$$\left(\bar{\alpha}_i \mathbf{I}_N + \sqrt{A}\right) \beta_i^\ell = \left(\bar{\alpha}_i \mathbf{I}_N - \sqrt{A}\right) \beta_j^{\ell-1}, \quad j = 3 - i, \quad \forall \ell \geq 2. \quad (4.14b)$$

For $i = 1, 2$, the matrix $\left(\bar{\alpha}_i \mathbf{I}_N + \sqrt{A}\right)$ is nonsingular. Indeed, using the Jordan decomposition of $\sqrt{A}$ given in (3.4), and that $\bar{\alpha}_i > 0$, we get

$$\det\left(\bar{\alpha}_i \mathbf{I}_N + \sqrt{A}\right) = \det\left(Q^{-1}(\bar{\alpha}_i \mathbf{I}_N + J_1)Q\right) = \det\left(\bar{\alpha}_i \mathbf{I}_N + J_1\right) = (\bar{\alpha}_i + 1)^N \neq 0.$$

[*] As all matrices of type $(\bar{\alpha}_i \mathbf{I}_N \pm \sqrt{A})$ and their inverses commute one with the other, matrix M is independent of indices i and j.

[**] Formulas (4.12a) and (4.13a) below are only well-defined for $\bar{\alpha}_j \neq 1,\ j = 1, 2$. If $\bar{\alpha}_j = 1$, for $j = 1$ or $j = 2$, we have, for $i = 3 - j$, the equality $\beta_i^{2\ell} = (M(\bar{\boldsymbol{\alpha}}))^{\ell-1} \beta_i^2$ and the convergence estimate $\frac{\|E_i^{2\ell}(0)\|_\infty}{\|E_i^2(0)\|_\infty} \leq \|(M(\bar{\boldsymbol{\alpha}}))^{\ell-1}\|_\infty,\ \forall \ell \geq 1$.

Thus, from (4.14a) and (4.14b) we obtain, for $i = 1, 2$,

$$\beta_i^2 = \left(\bar{\alpha}_i \mathbf{I}_N + \sqrt{A}\right)^{-1} \left(\bar{\alpha}_i \mathbf{I}_N - \sqrt{A}\right) \left(\bar{\alpha}_j \mathbf{I}_N + \sqrt{A}\right)^{-1} \bar{G}_j^0, \quad j = 3 - i, \tag{4.15a}$$

$$\beta_i^\ell = M(\bar{\boldsymbol{\alpha}}) \beta_i^{\ell-2}, \quad \forall \ell \geq 3. \tag{4.15b}$$

Multiplying now (4.15a) and (4.15b) by $(\bar{\alpha}_j \mathbf{I}_N - \sqrt{A})$, with $j = 3 - i$, then using that all matrices of type $(\bar{\alpha}_i \mathbf{I}_N \pm \sqrt{A})$ and their inverses commute one with the other, and using (4.9), we get, for $j = 1, 2$,

$$\begin{aligned} \bar{G}_j^2 &= M(\bar{\boldsymbol{\alpha}}) \bar{G}_j^0, \\ \bar{G}_j^\ell &= M(\bar{\boldsymbol{\alpha}}) \bar{G}_j^{\ell-2}, \quad \text{for } \ell \geq 3, \end{aligned}$$

from which (4.11) is deduced by induction. From (4.15b), we also get (4.12b) by induction. Then, taking the L^∞-norm of (4.12b), and using (4.5), we deduce (4.13b).

Let us now prove (4.12a) and (4.13a). We will distinguish the following cases :

Case $\bar{\alpha}_i \neq 1$, for $i = 1, 2$. Multiplying equations (4.11) by $(\bar{\alpha}_i \mathbf{I}_N - \sqrt{A})^{-1}$ and then using (4.7) and (4.9) lead to (4.12a). Then, taking the L^∞-norm of (4.12a), and using (4.5) and (4.8), we get (4.13a).

Case $\bar{\alpha}_i = 1$, for $i = 1$ or $i = 2$. In that case, relations (4.12a) and (4.13a) are replaced by $\beta_i^{2\ell} = (M(\bar{\boldsymbol{\alpha}}))^{\ell-1} \beta_i^2$ and $\frac{\|E_i^{2\ell}(0)\|_\infty}{\|E_i^2(0)\|_\infty} \leq \|(M(\bar{\boldsymbol{\alpha}}))^{\ell-1}\|_\infty$, $\forall \ell \geq 1$, respectively (see Footnote **). The first relation is obtained by induction from (4.15b). Then, taking its L^∞-norm, and using (4.5), we obtain the second one.

Let us now prove that Algorithm 4.1 converges. Matrix $\sqrt{A}$ is lower triangular with value 1 on the diagonal. Thus, $M(\bar{\boldsymbol{\alpha}})$ is a lower triangular matrix with a unique diagonal coefficient σ, that is its unique eigenvalue, given by

$$\sigma = \left(\frac{\bar{\alpha}_1 - 1}{\bar{\alpha}_1 + 1}\right) \left(\frac{\bar{\alpha}_2 - 1}{\bar{\alpha}_2 + 1}\right).$$

Thus the spectral radius of $M(\bar{\boldsymbol{\alpha}})$ is equal to $|\sigma|$ and strictly smaller than 1, as $\bar{\alpha}_i > 0$. Consequently, we have $\lim_{\ell \to \infty} (M(\bar{\boldsymbol{\alpha}}))^\ell = 0_{N,N}$, and thus $\lim_{\ell \to \infty} \beta_i^{2\ell} = \lim_{\ell \to \infty} \beta_i^{2\ell+1} = 0_N$, for $i = 1, 2$. Then $\lim_{\ell \to \infty} \|E_i^{2\ell}\|_{\boldsymbol{L}^\infty(\Omega_i)} = \lim_{\ell \to \infty} \|E_i^{2\ell+1}\|_{\boldsymbol{L}^\infty(\Omega_i)} = 0$, $i = 1, 2$, and $\lim_{\ell \to \infty} \|E_i^{2\ell}\|_{\boldsymbol{H}^1(\Omega_i)} = \lim_{\ell \to \infty} \|E_i^{2\ell+1}\|_{\boldsymbol{H}^1(\Omega_i)} = 0$, $i = 1, 2$, for all positive $\bar{\alpha}_1, \bar{\alpha}_2$, which proves the convergence of Algorithm 4.1. ∎

From Theorem 4.2, the following finite convergence results can be derived.

THEOREM 4.3 (Finite convergence of OSWR method). *Let $\bar{\alpha}_i$, $i = 1, 2$, be the dimensionless Robin parameters defined in (4.1).*

(i) If $\bar{\alpha}_1 = 1$ or $\bar{\alpha}_2 = 1$ (two-sided case), then the OSWR algorithm 4.1 converges in at most $2N + 2$ iterations;

(ii) If $\bar{\alpha}_1 = \bar{\alpha}_2 = 1$ (one-sided case), then the OSWR algorithm 4.1 converges in at most $N + 1$ iterations.

Proof. Let us prove (i). Using in (4.11a) the Jordan decomposition of $\sqrt{A}$ (given in (3.4)), we get, for $\ell \geq 0$, for $i = 1, 2$

$$\bar{G}_i^{2\ell} = Q^{-1} \left(\left(\bar{\alpha}_i \mathbf{I}_N + J_1\right)^{-1} \left(-\bar{\alpha}_i \mathbf{I}_N + J_1\right) \left(\bar{\alpha}_j \mathbf{I}_N + J_1\right)^{-1} \left(-\bar{\alpha}_j \mathbf{I}_N + J_1\right) \right)^\ell Q \, \bar{G}_i^0.$$

Using Property 3.6, the four matrices commute one with the other (as each matrix is a Jordan matrix, e.g. $\bar{\alpha}_i \mathbf{I}_N + J_1 = J_{1+\bar{\alpha}_i}$). Then, we have :

$$\bar{G}_i^{2\ell} = Q^{-1} \left(\bar{\alpha}_i \mathbf{I}_N + J_1\right)^{-\ell} \left(-\bar{\alpha}_i \mathbf{I}_N + J_1\right)^{\ell} \left(\bar{\alpha}_j \mathbf{I}_N + J_1\right)^{-\ell} \left(-\bar{\alpha}_j \mathbf{I}_N + J_1\right)^{\ell} Q\, \bar{G}_i^0. \quad (4.16)$$

Let $i = 1$ or $i = 2$, and $j = 3 - i$. Let $\bar{\alpha}_i = 1$ (and $\bar{\alpha}_j$ arbitrary). Then the matrix $-\bar{\alpha}_i \mathbf{I}_N + J_1$ has all its coefficients zero, except the superdiagonal ones. Thus, $-\bar{\alpha}_i \mathbf{I}_N + J_1$ is an $N \times N$ nilpotent matrix of index N. Consequently, from (4.16) with $\ell = N$, we have $\bar{G}_i^{2N} = 0_N$. Using now relation (4.14b), which is written

$$\beta_i^{\ell+1} = \left(\bar{\alpha}_i \mathbf{I}_N + \sqrt{A}\right)^{-1} \left(\bar{\alpha}_i \mathbf{I}_N - \sqrt{A}\right) \beta_j^{\ell} = \left(\bar{\alpha}_j \mathbf{I}_N + \sqrt{A}\right)^{-1} \bar{G}_i^{\ell},$$

we obtain $\beta_i^{2N+1} = 0_N$, and with (4.14b) we also have

$$\beta_j^{\ell+2} = \left(\bar{\alpha}_j \mathbf{I}_N + \sqrt{A}\right)^{-1} \left(\bar{\alpha}_j \mathbf{I}_N - \sqrt{A}\right) \beta_i^{\ell+1},$$

thus $\beta_j^{2N+2} = 0_N$. Finally, from (4.5), we get $E_i^{2N+2} = 0_N$, $i = 1, 2$.

Let us now prove (ii). Taking $\bar{\alpha}_1 = \bar{\alpha}_2 = 1$ and multiplying both equations of (4.14) by $(\mathbf{I}_N - \sqrt{A})$, one gets :

$$\bar{G}_j^1 = \left(\mathbf{I}_N + \sqrt{A}\right)^{-1} \left(\mathbf{I}_N - \sqrt{A}\right) \bar{G}_i^0,$$
$$\bar{G}_j^{\ell} = \left(\mathbf{I}_N + \sqrt{A}\right)^{-1} \left(\mathbf{I}_N - \sqrt{A}\right) \bar{G}_i^{\ell-1}, \quad j = 3 - i, \quad \forall \ell \geq 2.$$

Thus, by induction, we obtain

$$\bar{G}_j^{\ell} = \left(\mathbf{I}_N + \sqrt{A}\right)^{-\ell} \left(\mathbf{I}_N - \sqrt{A}\right)^{\ell} \bar{G}_{i/j}^0,$$

where $\bar{G}_{i/j}^0$ is $\bar{G}_j^0$ if ℓ is even, $\bar{G}_i^0$ is ℓ is odd.
Using the Jordan decomposition of $\sqrt{A}$ in the above equality (as in (i)), we get

$$\bar{G}_j^{\ell} = Q^{-1} (\mathbf{I}_N + J_1)^{-\ell} (\mathbf{I}_N - J_1)^{\ell} Q \bar{G}_{i/j}^0.$$

Then, if $\ell = N$, one gets that $\bar{G}_j^N = 0$, $j = 1, 2$, and thus, using (4.14b) and (4.9), we get $\beta_j^{N+1} = (\mathbf{I}_N + \sqrt{A})^{-1} (\mathbf{I}_N - \sqrt{A}) \beta_i^N = (\mathbf{I}_N + \sqrt{A})^{-1} \bar{G}_j^N = 0_N$, $j = 1, 2$. Finally, from (4.5), we have $E_j^{N+1} = 0_N$, for $j = 1, 2$. ∎

From Theorem 4.2, the following result can be obtained.

THEOREM 4.4 (Convergence depending only on $\bar{\boldsymbol{\alpha}}$). *For a given $N \geq 1$, the L^∞-norm convergence of Algorithm 4.1 depends only on $\bar{\boldsymbol{\alpha}}$.*

Proof. This result directly comes from (4.12) where M depends only on $\bar{\boldsymbol{\alpha}}$ and on N through its dimension. Indeed, the convergence of the sequence $(\beta_i^{\ell})_{\ell \in \mathbb{N}}$, $i = 1, 2$, depends only on $\bar{\boldsymbol{\alpha}}$ and N. Then, using (4.5) and that $\|E_i^{\ell}\|_{\boldsymbol{L}^\infty(\Omega_i)} = \|\beta_i^{\ell}\|_\infty$ $i = 1, 2$, the theorem is proven. ∎

Remark 4.5. For a given $N \geq 1$ (and thus for a given Δt), once the choice of $\bar{\boldsymbol{\alpha}} = (\bar{\alpha}_1, \bar{\alpha}_2)$ has been performed as recommended in Section 4.5 below, one simply has to choose $\alpha_i = \bar{\alpha}_i \sqrt{\frac{\nu}{\Delta t}}$, $i = 1, 2$, to obtain an efficient convergence which will not depend on ν (as follows from Theorem 4.4).

Remark 4.6 (Notation for matrix M). Throughout the sequel of this paper, the matrix defined in (4.10) will be denoted by $M(\bar{\alpha})$ in the one-sided case $\bar{\boldsymbol{\alpha}} = (\bar{\alpha}, \bar{\alpha})$, and by $M(\bar{\boldsymbol{\alpha}})$ in the two-sided case $\bar{\boldsymbol{\alpha}} = (\bar{\alpha}_1, \bar{\alpha}_2)$.

Remark 4.7. Note that in (4.13), one could use the upper bound

$$\|(M(\bar{\boldsymbol{\alpha}}))^{\ell}\|_{\infty} \leq \|M(\bar{\boldsymbol{\alpha}})\|_{\infty}^{\ell}, \tag{4.17}$$

and then define Robin parameters, for the one-sided and two-sided cases, respectively denoted by $\bar{\alpha}_M$ and $\bar{\boldsymbol{\alpha}}_M$, as follows[‡]

$$\|M(\bar{\alpha}_M)\|_{\infty} = \min_{\bar{\alpha}\in]0,1]} \|M(\bar{\alpha})\|_{\infty}, \qquad \|M(\bar{\boldsymbol{\alpha}}_M)\|_{\infty} = \min_{\bar{\boldsymbol{\alpha}}\in]0,1]^2} \|M(\bar{\boldsymbol{\alpha}})\|_{\infty}. \tag{4.18}$$

However, for a given $N \geq 1$, $\|M(\bar{\boldsymbol{\alpha}}_M)\|_{\infty}^{\ell}$ is larger and closer to 1 than $\|(M(\bar{\boldsymbol{\alpha}}_M))^{\ell}\|_{\infty}$, and differs more and more from $\|(M(\bar{\boldsymbol{\alpha}}_M))^{\ell}\|_{\infty}$ when ℓ increases. Thus one loses information in the use of the upper bound (4.17). This will be observed numerically in Section 5.6, where the convergence with $\bar{\boldsymbol{\alpha}}_M$ is much slower (except for the very first iterations) than that with the parameter $\bar{\boldsymbol{\alpha}}$ that minimizes $\|(M(\bar{\boldsymbol{\alpha}}))^{\ell}\|_{\infty}$. Consequently, one main objective of this article is to search for discrete-time optimized Robin parameters $\bar{\boldsymbol{\alpha}} = \bar{\boldsymbol{\alpha}}(\ell)$, that depend on iteration ℓ, and minimize $\|(M(\bar{\boldsymbol{\alpha}}))^{\ell}\|_{\infty}$. Such parameters will be defined in Section 4.5.

Remark 4.8 (Equivalent writing of discrete-time estimate and notation). From relations (4.13), the discrete-time estimates at iteration ℓ read

$$\frac{\|E_i^{\ell}(0)\|_{\infty}}{\|E_i^{0}(0)\|_{\infty}} \leq \|(M(\bar{\boldsymbol{\alpha}}))^{q(\ell)}\|_{\infty}, \quad \forall \ell \geq 0 \text{ even}, \tag{4.19a}$$

$$\frac{\|E_i^{\ell}(0)\|_{\infty}}{\|E_i^{1}(0)\|_{\infty}} \leq \|(M(\bar{\boldsymbol{\alpha}}))^{q(\ell)}\|_{\infty}, \quad \forall \ell \geq 1 \text{ odd}, \tag{4.19b}$$

$$\text{with} \quad q(\ell) := \begin{cases} \frac{\ell}{2} & \text{if} \quad \ell \text{ is even} \\ \frac{\ell-1}{2} & \text{if} \quad \ell \text{ is odd} \end{cases}, \quad \forall \ell \geq 0. \tag{4.20}$$

Thus, $\|(M(\bar{\boldsymbol{\alpha}}))^{q(\ell)}\|_{\infty}$ is an estimate of the relative L^{∞}-error at iteration ℓ, for $\ell \geq 0$.

4.5. Choice of the Robin parameters. Let us first consider the one-sided case, i.e. $\bar{\alpha} := \bar{\alpha}_1 = \bar{\alpha}_2$. The convergence matrix defined in (4.10) then reads

$$M(\bar{\alpha}) = \left(\left(\bar{\alpha}\mathbf{I}_N + \sqrt{A} \right)^{-1} \left(\bar{\alpha}\mathbf{I}_N - \sqrt{A} \right) \right)^2, \quad i = 1, 2.$$

Remarks 4.7 and 4.8 lead us to define a *discrete-time optimized Robin parameter*, denoted by $\bar{\alpha}_{D[\ell]}$, depending on iteration $\ell \geq 2$, as follows[‡]

$$\|(M(\bar{\alpha}_{D[\ell]}))^{q(\ell)}\|_{\infty} = \min_{\bar{\alpha}\in]0,1]} \|(M(\bar{\alpha}))^{q(\ell)}\|_{\infty}, \tag{4.21}$$

where $q(\ell)$ is defined in (4.20).
For example, if one wants to optimize the convergence at iteration $\ell = 7$, then one can use the Robin parameter $\bar{\alpha}_{D[7]}$ such that $\|M(\bar{\alpha}_{D[7]})\|_{\infty} = \min_{\bar{\alpha}\in]0,1]} \|(M(\bar{\alpha}))^3\|_{\infty}$.

[‡]The choice of the interval $]0, 1]$ in the minimization problem comes from the fact that the Robin parameters are positive, and from our numerical observations in Section 5.3.

Remark 4.9. In practice, for the minimization problem in (4.21), we calculate $\|(M(\gamma_j))^{q(\ell)}\|_\infty$, with $\gamma_j := \frac{j}{100}$ for $j \in [\![1, 100]\!]$, then take the index j_0 that gives the minimum value, and set $\bar{\alpha}_{D[\ell]} = \gamma_{j_0}$.

Note that, although this process requires the repeated inversion of matrices, its cost remains low for the following reasons :

- the matrices are of size N and thus remain of moderate size, since for long time computations a splitting of the time interval into windows is necessary, and one uses the OSWR method in each time window [4, 23];
- the matrices involved at iteration ℓ will be recycled for iteration $\ell + 1$, so that the marginal cost of computing the norms of the matrices for an extra iteration remains cheap;
- the calculation of the terms $\|(M(\gamma_j))^{q(\ell)}\|_\infty,\ j \in [\![1, 100]\!]$, can be completely parallelized (with respect to j);
- the method provides a dimensionless optimized parameter $\bar{\alpha}_{D[\ell]}$ whose dependency is only in ℓ and N, and thus independent of the other parameters ν, f, u_0 and of space discretization. It can therefore be calculated only once, at fixed N, whatever the other data of the problem. The (dimensional) optimized Robin parameter is then given by $\alpha_{D[\ell]} := \sqrt{\frac{\nu}{\Delta t}}\bar{\alpha}_{D[\ell]}$.

This process can be extended to the two-sided case with corresponding *two-sided discrete-time optimized parameters* denoted by $\bar{\boldsymbol{\alpha}}_{D[\ell]} = (\bar{\alpha}_{1,D[\ell]}, \bar{\alpha}_{2,D[\ell]})$, as follows :

$$\|(M(\bar{\boldsymbol{\alpha}}_{D[\ell]}))^{q(\ell)}\|_\infty = \min_{\bar{\boldsymbol{\alpha}} \in]0,1]^2} \|(M(\bar{\boldsymbol{\alpha}}))^{q(\ell)}\|_\infty, \tag{4.22}$$

where $M(\bar{\boldsymbol{\alpha}})$ is defined in (4.10).

Remark 4.10. Note that, by definition of $\bar{\alpha}_M$ and $\bar{\boldsymbol{\alpha}}_M$ in (4.18), and of $\bar{\alpha}_{D[\ell]}$ and $\bar{\boldsymbol{\alpha}}_{D[\ell]},\ \ell \geq 2$, in (4.21) and (4.22) respectively, we have the following relations :

$$\bar{\alpha}_M = \bar{\alpha}_{D[2]} = \bar{\alpha}_{D[3]}, \qquad \bar{\boldsymbol{\alpha}}_M = \bar{\boldsymbol{\alpha}}_{D[2]} = \bar{\boldsymbol{\alpha}}_{D[3]}.$$

5. Numerical results. In this section, some numerical experiments are presented to illustrate the theoretical results of Section 4.

The domain $\Omega = [0, 1]$ is of length $L = 1$. The resolution is done using a finite element code developed in the GNU Octave [10] language, whose mesh size is $\Delta x = 10^{-3}$ (except in Section 5.5 where $\Delta x = 5 \times 10^{-5}$). The final time is $T = 1$, and the time step is $\Delta t = \frac{T}{N}$, where N will vary, depending on the numerical examples.

In our test cases we simulate the error equations, i.e. we take $u_0 = 0$ and $f = 0$. As the domain is now bounded, we add homogeneous Dirichlet conditions at $x = 0$ and $x = 1$.

We use the OSWR algorithm with the interface at $x = \frac{1}{2}$, and with random initial Robin data on the interface so that all the frequency components are present. The algorithm is stopped when the L^∞-norm of the jump of the Robin transmission conditions on the interface is smaller than 10^{-10}, unless specified.

In Section 4.4 we have proved that the convergence of the discrete-time OSWR algorithm depends only on dimensionless Robin parameters $\bar{\boldsymbol{\alpha}} = (\bar{\alpha}_1, \bar{\alpha}_2)$ and on N. Thus, in what follows, we will consider only dimensionless Robin parameters $\bar{\alpha}_1, \bar{\alpha}_2$.[§]

The solution of the fully discrete error equations at iteration ℓ is denoted $E^\ell_{i,\Delta x}$, and is measured, on the interface[†], either in the L^∞-norm, or in the L^∞-norm scaled

[§]This means that in the OSWR algorithm we take $\alpha_i = \bar{\alpha}_i\sqrt{\frac{\nu}{\Delta t}},\ i = 1, 2$.

[†]Similar results will be obtained if one takes the maximum of the L^∞-errors in the subdomains.

by the initial error, as in our theoretical result (4.19b).¶

In what follows, we will use the following terms, that are associated to the OSWR iteration ℓ (excepted for the first item in the list bellow)

- *continuous optimized Robin parameter(s)* : $\bar{\alpha}_C$ or $\bar{\boldsymbol{\alpha}}_C$ given in (4.2)
- *fully discrete numerical solution* : $E^{\ell}_{i,\Delta x}$ (as defined above)
- L^∞*-error* : error term $\|E^{\ell}_{i,\Delta x}(0)\|_\infty$
- *relative* L^∞*-error* : error term $\frac{\|E^{\ell}_{i,\Delta x}(0)\|_\infty}{\|E^{1}_{i,\Delta x}(0)\|_\infty}$
- *discrete-time convergence estimate* : upper bound $\|(M(\bar{\boldsymbol{\alpha}}))^{q(\ell)}\|_\infty$ in (4.19)
- *discrete-time optimized Robin parameter(s)* : $\bar{\alpha}_{D[\ell]}$ or $\bar{\boldsymbol{\alpha}}_{D[\ell]}$, see Section 4.5

Since the problem is symmetrical for the two domains, the results presented here are only for the left domain (similar results will be obtained for the right domain, up to a permutation of α_1 and α_2 in the two-sided case).

Remark 5.1. While our analysis has been carried out on an infinite domain, in practice, the fully discrete numerical solution is necessarily calculated on a bounded domain. However, we can show that the theory is not very much affected by the bounded domain, as long as $\sqrt{\nu\Delta t} \ll L$. Indeed, on a bounded domain, the solution is not exactly (4.5) but will involve matrices $\mathrm{e}^{\frac{-|x|}{\sqrt{\nu\Delta t}}\sqrt{A}}$ and $\mathrm{e}^{\frac{|x|}{\sqrt{\nu\Delta t}}\sqrt{A}}$ (as shown below in (6.2)), and the norm of the vector coefficient associated to the latter will become very small if $\sqrt{\nu\Delta t} \ll L$. Thus, in our fully discrete numerical experiments, ν, Δt and L have been chosen so that they verify this condition.

Remark 5.2. As our analysis has been carried out in the semi-discrete in time case, we will take Δx small enough in the numerical experiments, to approach the discrete-time problem, i.e. we take $\Delta x \ll \sqrt{\nu\Delta t}$. However, when the previous condition is not satisfied, e.g. when $\Delta x = \Delta t$, we get similar numerical results.

Section 5.1 illustrates that, for a given $N \geq 1$, the convergence depends only on $\bar{\boldsymbol{\alpha}}$. Then, in Section 5.2, we verify that, at each OSWR iteration, the discrete-time convergence estimate is an accurate evaluation of the relative L^∞-error. Sections 5.3 and 5.4 illustrate the importance of choosing Robin parameters that are optimized for a targeted iteration count. In Section 5.5, asymptotic behaviors as a function of N are shown. Finally in Section 5.6, a comparison with $\bar{\alpha}_M$ and $\bar{\boldsymbol{\alpha}}_M$ (defined in (4.18)) is given.

In Sections 5.1 to 5.3 we consider one-sided Robin parameters $\bar{\alpha} \coloneqq \bar{\alpha}_1 = \bar{\alpha}_2$. The case of two-sided parameters ($\bar{\alpha}_1$ and $\bar{\alpha}_2$ possibly different) will be treated in Section 5.4, and both cases will be considered in Sections 5.5 and 5.6.

5.1. Convergence depending only on $\bar{\boldsymbol{\alpha}}$, for a given N. In this part we take $N = 100$. From Theorem 4.4 and Remark 4.5, we expect, for a fixed $\bar{\alpha}$, a convergence almost independent of ν when α is chosen as $\alpha = \bar{\alpha}\sqrt{\frac{\nu}{\Delta t}}$.

In Figure 1, we plot the evolution of the L^∞-error as a function of the number of iterations, for three values of ν (0.1, 0.05, 0.01). The four graphs correspond to four values of $\bar{\alpha}$ (0.1, 0.5, 1 and 3). We observe that the convergence is not influenced by the diffusion coefficient ν, as expected. As a consequence, in what follows, we only consider the case $\nu = 0.05$.

¶One could also consider a scaling by $\|E^0_i(0)\|_\infty = \|\beta^0_i\|_\infty$ as in (4.19a), which will lead to similar results, if one takes random values for β^0_i, and then set $G^0_i \coloneqq (\bar{\alpha}_i \mathbf{I}_N - \sqrt{A})\beta^0_j,\ j = 3-i,\ i = 1, 2$.

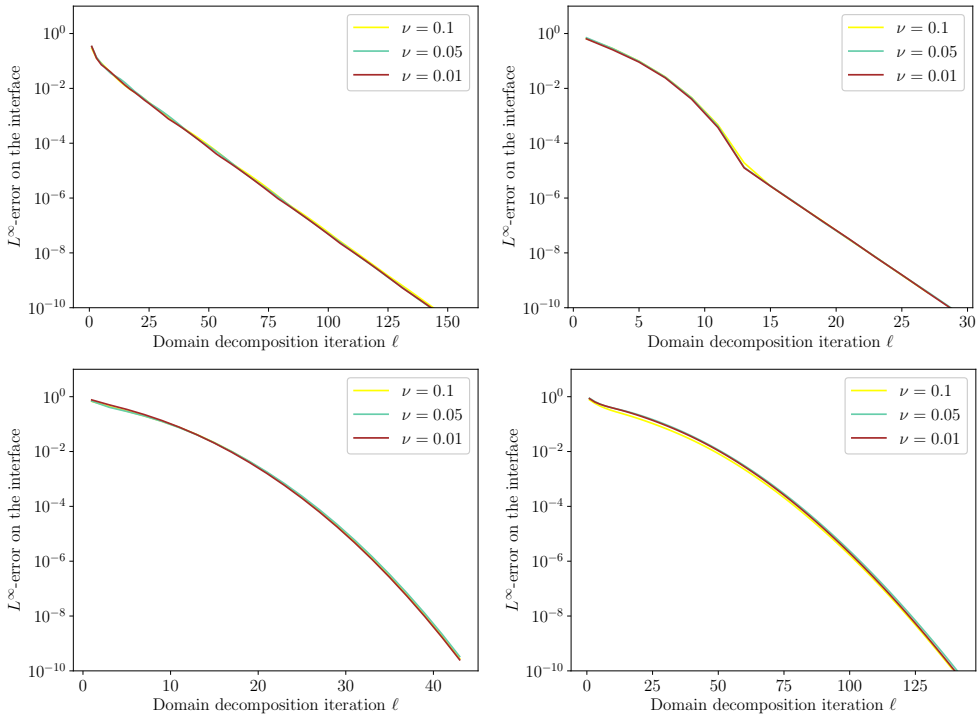

FIG. 1. *Illustration of convergence, which only depends on $\bar{\alpha}$, for a fixed N : L^∞-error, with $N = 100$ and different values of ν, for $\bar{\alpha} = 0.1$ (top left), $\bar{\alpha} = 0.5$ (top right), $\bar{\alpha} = 1$ (bottom left), $\bar{\alpha} = 3$ (bottom right).*

5.2. Comparison between discrete-time estimate and relative L^∞-error. In this part, we show that the discrete-time convergence estimate $\|(M(\bar{\alpha}))^{q(\ell)}\|_\infty$ in (4.19) approaches well the relative L^∞-error, at each OSWR iteration ℓ, which confirms the interest of the theoretical analysis.

In Figure 2, we plot the relative L^∞-error (solid line) and the discrete-time estimate (dashed line), as functions of the number of iterations, for $N = 100$, and for different values of $\bar{\alpha}$ (0.1, 0.5, 1 and 3).

We observe that the discrete-time estimate is an upper bound of the relative L^∞-error, as expected from (4.19). Thus, we could not expect both curves to exactly overlay. However, the discrete-time estimates closely follow the actual relative L^∞-error curves, and even closer when $\bar{\alpha}$ is larger. A possible explanation for the differences is that the theoretical analysis of this paper is done on an infinite domain, while the numerical results are performed on the bounded domain $[0, 1]$. Another possible explanation is the loss of information when going from equalities (4.12) to inequalities (4.13).

Consequently, this observation makes it relevant to find optimized dimensionless Robin parameters that minimize the discrete-time estimate, as done in Section 4.5. In the following subsections, we show numerical results on the influence of such Robin parameters.

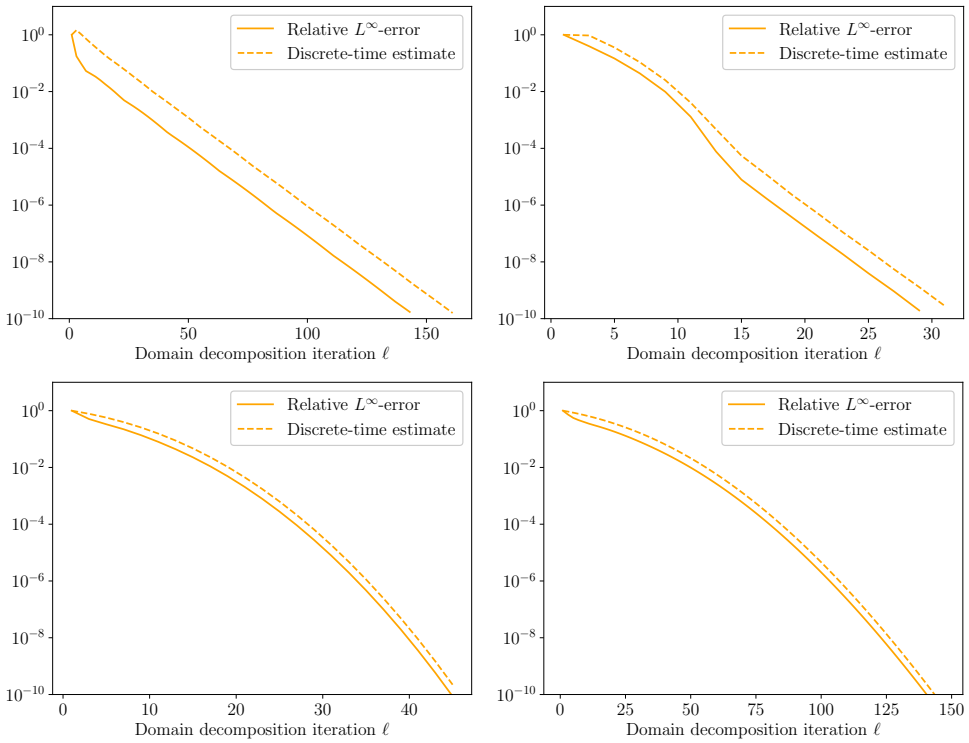

FIG. 2. *Comparison of relative L^∞-error (solid line) and discrete-time estimate (dashed line), for $N = 100$, with $\bar{\alpha} = 0.1$ (top left), $\bar{\alpha} = 0.5$ (top right), $\bar{\alpha} = 1$ (bottom left), $\bar{\alpha} = 3$ (bottom right).*

5.3. One-sided optimization. In this part, we consider *one-sided* Robin parameters ($\bar{\alpha}_1 = \bar{\alpha}_2$). We compute $\bar{\alpha}_{D[\ell]}$ using the method described in Remark 4.9.

Figure 3 shows, for different values of N, the values of $\bar{\alpha}_{D[\ell]}$ as a function of the targeted iteration count ℓ (left figure), and the associated discrete-time estimate $\|(M(\bar{\alpha}_{D[\ell]}))^{q(\ell)}\|_\infty$ versus iteration ℓ (right figure).

ABACUS 5.3 (How to choose ℓ and $\bar{\alpha}$ to reach a given accuracy). *Figure 3 allows to find an optimized pair $(\bar{\alpha}_{D[\ell]}, \ell)$ to reach a given accuracy, e.g. the expected accuracy of the numerical scheme, or a fraction thereof. More precisely, the right figure enables, for a given N, to find the minimum number ℓ of iterations one has to perform in order to reach a given error. Then, the left figure gives the associated Robin parameter $\bar{\alpha}_{D[\ell]}$.*

For example, in the case $N = 20$, if one wants to guarantee a relative L^∞-error smaller than 10^{-2}, then from Figure 3 (right) one only needs to perform seven iterations ($\ell = 7$). Then Figure 3 (left) gives the discrete-time optimized Robin parameter $\bar{\alpha}_{D[7]} = 0.68$.

With the cases $N = 20$ and $N = 50$, we see that for $\ell \geq N$ iterations, the discrete-time optimized Robin parameter is 1, as expected from Theorem 4.3. These numerical results also show that, after a few iterations, $\bar{\alpha}_{D[\ell]}$ is a globally increasing function of ℓ, that tends to 1, and a decreasing function of N.

Let us now compare the convergence obtained with the discrete-time optimized parameter $\bar{\alpha}_{D[\ell]}$ to that obtained with the continuous optimized parameter $\bar{\alpha}_C$ defined in (4.2). For this, we will consider $\bar{\alpha}_{D[\ell]}$ at two different iterations : $\ell = 7$ and $\ell = 21$.

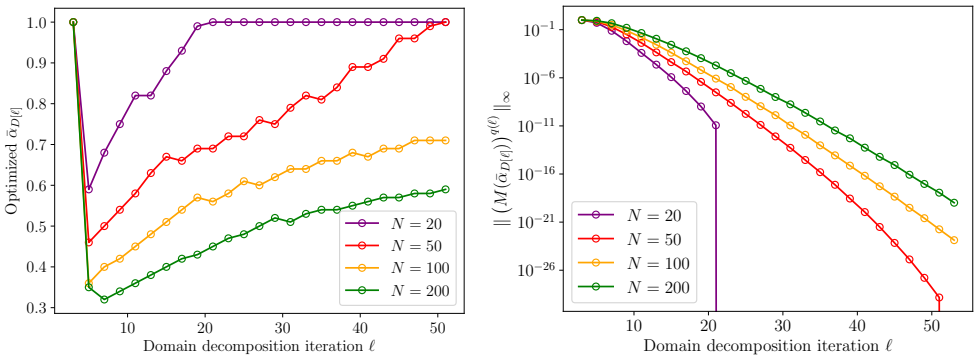

FIG. 3. *Discrete-time optimized Robin parameter $\bar{\alpha}_{D[\ell]}$ (left) and associated discrete-time convergence estimate $\|(M(\bar{\alpha}_{D[\ell]}))^{q(\ell)}\|_\infty$ (right), versus OSWR iterations.*

The values of $\bar{\alpha}_C$ (rounded to the nearest hundredth), $\bar{\alpha}_{D[7]}$, and $\bar{\alpha}_{D[21]}$, versus N, are reported in Table 1.

N	$\bar{\alpha}_C$	$\bar{\alpha}_{D[7]}$	$\bar{\alpha}_{D[21]}$
20	0.84	0.68	1.00
50	0.67	0.50	0.69
100	0.56	0.40	0.56
200	0.47	0.32	0.45

TABLE 1

Dimensionless one-sided Robin parameter optimized with continuous and discrete-time analysis.

Recall that $\bar{\alpha}_C$ is independent of the iterations, while $\bar{\alpha}_{D[7]}$ and $\bar{\alpha}_{D[21]}$ optimize iterations 7 and 21, respectively. On Figure 4, we plot the L^∞-error as a function of OSWR iterations (note the scale change for the top left figure), for different values of N, and with $\bar{\alpha}_C$, $\bar{\alpha}_{D[7]}$, and $\bar{\alpha}_{D[21]}$. A horizontal line representing the scheme error (between the fully discrete monodomain solution and the continuous solution of (2.1), when the latter is $u(x,t) = (t^2+1)\sin(\pi x)$) in L^∞-norm is also drawn, and is the objective to be reached in order to add no significant error through domain decomposition. The scheme error values ε_{sch} are given in Table 2.

N	20	50	100	200
ε_{sch}	6×10^{-2}	2.5×10^{-2}	1.2×10^{-2}	6×10^{-3}

TABLE 2

L^∞-error of the fully discrete numerical scheme on the interface, as a function of N.

We observe that, for each N, the scheme error is reached sooner with $\bar{\alpha}_{D[7]}$ than with $\bar{\alpha}_C$ (e.g. for $N = 200$, reaching $\varepsilon_{sch} = 6 \times 10^{-3}$ needs 9 iterations with $\bar{\alpha}_{D[7]}$ and 13 with $\bar{\alpha}_C$). We also see that at iteration 7 (resp. 21), the L^∞-error with $\bar{\alpha}_{D[7]}$ (resp. $\bar{\alpha}_{D[21]}$) is smaller than the ones obtained with $\bar{\alpha}_C$ and $\bar{\alpha}_{D[21]}$ (resp. $\bar{\alpha}_{D[7]}$). This confirms the relevance of choosing an optimized parameter that depends on the targeted iteration, as pointed out by the analysis.

While the usual approach based on Fourier transform on continuous equations

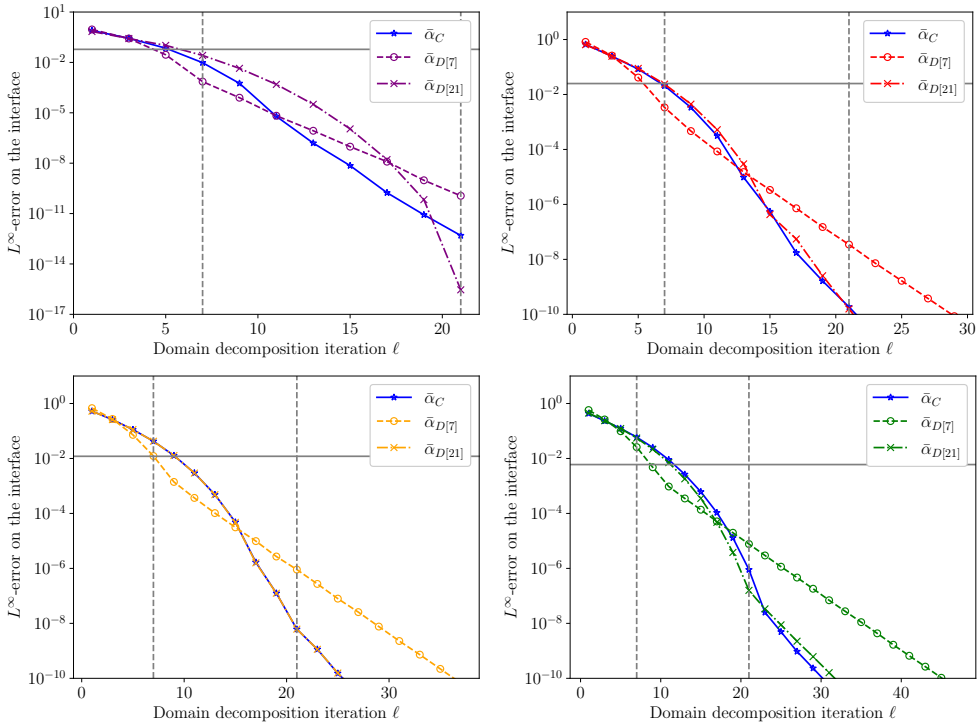

FIG. 4. *L^∞-error computed with one-sided continuous and discrete-time (optimized at iteration $\ell = 7$ and 21) Robin parameter, for $N = 20$ (top left), $N = 50$ (top right), $N = 100$ (bottom left), $N = 200$ (bottom right). Note the scale change for the top left figure (in that case convergence with $\bar{\alpha}_{D[21]} = 1$ is almost exact at the 21^{st} iteration, as expected from Theorem 4.3).*

gives optimized continuous Robin parameters that are independent of domain decomposition iterations, numerical results show that there is no single optimal coefficient, but rather an optimal $\bar{\alpha}(\ell)$ for each iteration ℓ. In particular, we observe that a Robin coefficient can be optimal at one iteration, but perform poorly at another. Optimization should then be carried out more accurately, iteration by iteration.

Let us now compare the continuous and discrete-time optimized Robin parameters to the actual numerical optimal ones. On Figure 5, we plot the relative L^∞-error at iteration 7 (left) and at iteration 21 (right) versus the Robin parameter $\bar{\alpha}$. On these graphs, stars stand for continuous optimized Robin parameters $\bar{\alpha}_C$, and triangles are discrete-time optimized Robin parameters $\bar{\alpha}_{D[7]}$ (left) and $\bar{\alpha}_{D[21]}$ (right). We see that, for all values of N, at iteration 7 (left figure) the parameter $\bar{\alpha}_{D[7]}$ is close to the numerical optimal $\bar{\alpha}$, and at iteration 21 (right figure) the parameter $\bar{\alpha}_{D[21]}$ is extremely close to the numerical optimal $\bar{\alpha}$. On Figure 5, we also observe that at iteration 21, the parameter $\bar{\alpha}_C$, obtained by the continuous framework, is also very close to the numerical optimal $\bar{\alpha}$, for $N = 50$ and $N = 100$. However, at iteration 21 for $N = 20$ and $N = 200$, and at iteration 7, for all N, the parameter $\bar{\alpha}_C$ is a worse approximation of the numerical optimal parameter than parameters obtained with the discrete-time method. This observation is crucial when one wants to perform a small number of iterations: in that case, the continuous optimization provides only a poor Robin coefficient and thus does not allow the OSWR algorithm to work efficiently.

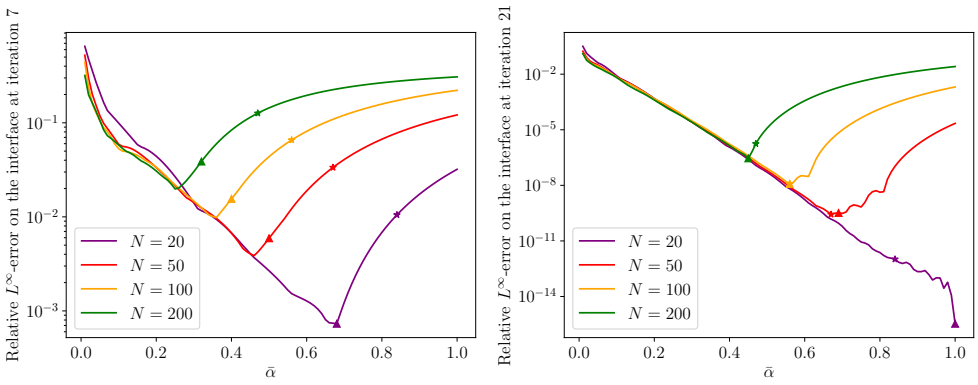

FIG. 5. *Relative L^∞-error on the interface as a function of $\bar{\alpha}$, at iteration 7 (left) and 21 (right). In each case, the triangles show $\bar{\alpha}_{D[7]}$ (left) and $\bar{\alpha}_{D[21]}$ (right), and the stars show $\bar{\alpha}_C$.*

One of the main results of this article is that there is not a single Robin coefficient, independent of the iterations, that optimizes each iteration. Figure 5 is an example that illustrates this point : the numerical optimum varies according to ℓ; the parameter α_C, that minimizes the continuous convergence factor (which is independent of the iteration), cannot optimize all iterations, whereas the method presented here allows to find a quite accurate approximation of the numerical optimum parameter, for each iteration ℓ.

5.4. Two-sided optimization. We now consider two-sided Robin parameters (i.e. $\bar{\alpha}_1$ and $\bar{\alpha}_2$ are possibly different). On Figure 6 we plot the L^∞-error as a function of OSWR iterations (note the scale change for the top left figure), obtained with the following optimized Robin parameters :

- continuous $\bar{\boldsymbol{\alpha}}_C = (\bar{\alpha}_{1,C}, \bar{\alpha}_{1,C})$, defined in (4.2) (independent of the iterations)
- discrete-time $\bar{\boldsymbol{\alpha}}_{D[7]}$ that optimizes iteration 7, defined in (4.22) with $\ell = 7$
- discrete-time $\bar{\boldsymbol{\alpha}}_{D[21]}$ that optimize iteration 21, defined in (4.22) with $\ell = 21$

Table 3 shows these values versus N (rounded to the nearest hundredth for $\bar{\boldsymbol{\alpha}}_C$).

N	$\bar{\boldsymbol{\alpha}}_C$	$\bar{\boldsymbol{\alpha}}_{D[7]}$	$\bar{\boldsymbol{\alpha}}_{D[21]}$
20	(0.56,1.26)	(0.55,0.86)	(1.00,1.00)
50	(0.30,1.49)	(0.33,0.80)	(0.68,0.70)
100	(0.21,1.46)	(0.23,0.74)	(0.48,0.66)
200	(0.17,1.33)	(0.16,0.77)	(0.30,0.69)

TABLE 3

Dimensionless two-sided Robin parameters optimized with continuous and discrete-time analysis.

As in the one-sided case, we observe that, for all values of N, the smallest L^∞-error is the one associated with the coefficient $\bar{\boldsymbol{\alpha}}_{D[7]}$ (resp. $\bar{\boldsymbol{\alpha}}_{D[21]}$) at iteration 7 (resp. 21). At iteration 7, the parameter $\bar{\boldsymbol{\alpha}}_C$ is a little less efficient than the discrete-time optimized parameter $\bar{\boldsymbol{\alpha}}_{D[7]}$. However, for a larger number of iterations (e.g. $\ell = 21$), $\bar{\boldsymbol{\alpha}}_C$ appears to be significantly less efficient than the discrete-time optimized parameter $\bar{\boldsymbol{\alpha}}_{D[21]}$. Again, we observe that the discrete-time optimized Robin coefficients proposed in this article allow to optimize efficiently the L^∞-error at a targeted iteration.

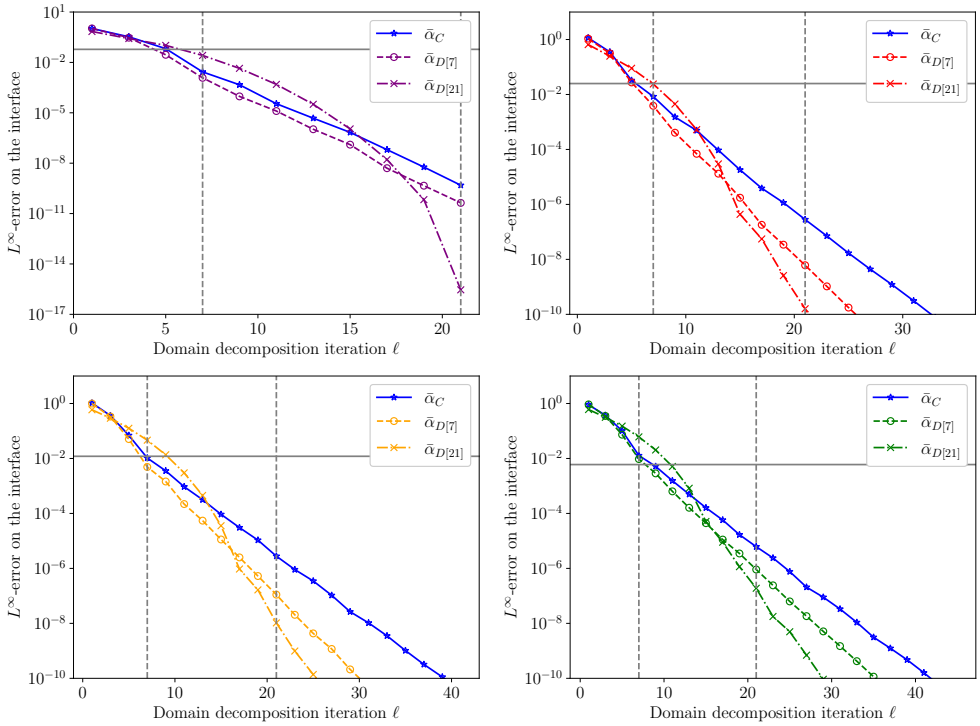

FIG. 6. *L^∞-error computed with two-sided continuous and discrete-time (optimized at iteration $\ell = 7$ and 21) Robin parameters, for $N = 20$ (top left), $N = 50$ (top right), $N = 100$ (bottom left), $N = 200$ (bottom right). Note the scale change for the top left figure, as explained in Figure 4.*

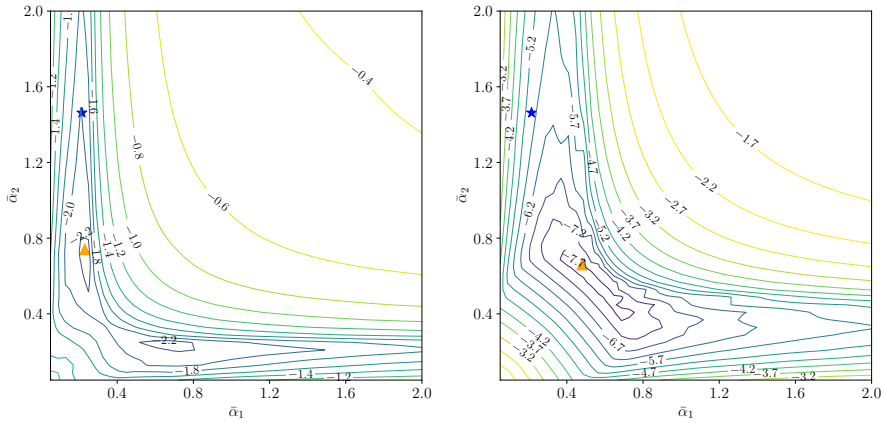

FIG. 7. *Level curves for the relative L^∞-error (in logarithmic scale) after 7 iterations (left), and 21 iterations (right), for various values of the parameters $\bar{\boldsymbol{\alpha}} = (\bar{\alpha}_1, \bar{\alpha}_2)$, for $N = 100$. The blue star shows $\bar{\boldsymbol{\alpha}}_C$, and the orange triangle shows $\bar{\boldsymbol{\alpha}}_{D[7]}$ (left) and $\bar{\boldsymbol{\alpha}}_{D[21]}$ (right).*

On Figure 7, we plot the level curves for the relative L^∞-error (in logarithmic scale) after 7 iterations (left), and 21 iterations (right), for various values of the two-sided Robin parameters $\bar{\boldsymbol{\alpha}} = (\bar{\alpha}_1, \bar{\alpha}_2)$, for $N = 100$. The blue star shows the

continuous optimized parameter $\bar{\boldsymbol{\alpha}}_C$, and the orange triangle shows the discrete-time optimized parameter $\bar{\boldsymbol{\alpha}}_{D[7]}$ (left figure) and $\bar{\boldsymbol{\alpha}}_{D[21]}$ (right figure). We observe that, at iteration 7 (resp. 21), the discrete-time optimized parameter $\bar{\boldsymbol{\alpha}}_{D[7]}$ (resp. $\bar{\boldsymbol{\alpha}}_{D[21]}$) is close to the numerical optimal $\bar{\boldsymbol{\alpha}}$, and much closer to this optimal value than $\bar{\boldsymbol{\alpha}}_C$.

Moreover, we notice that, the higher the number ℓ of domain decomposition iterations, the less $\bar{\alpha}_{1,D[\ell]}$ and $\bar{\alpha}_{2,D[\ell]}$ differ, as shown on Figure 8.

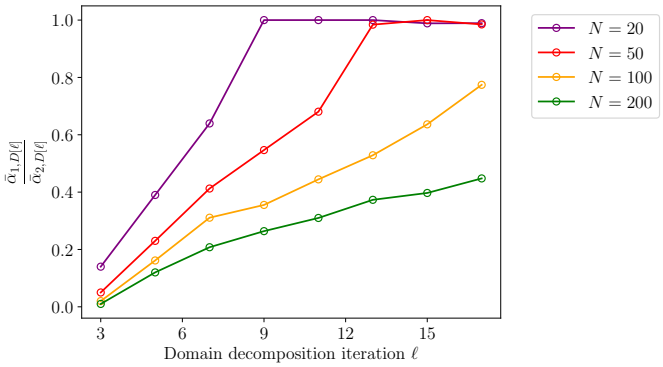

FIG. 8. *Ratio between discrete-time optimized two-sided Robin coefficients.*

5.5. Asymptotic behavior as a function of N. In this part, we present the asymptotic performance, with continuous and discrete-time optimized parameters. In Figure 9 we take $\Delta x = 5 \times 10^{-5}$, and plot the number $\ell_\star$ of iterations that it takes

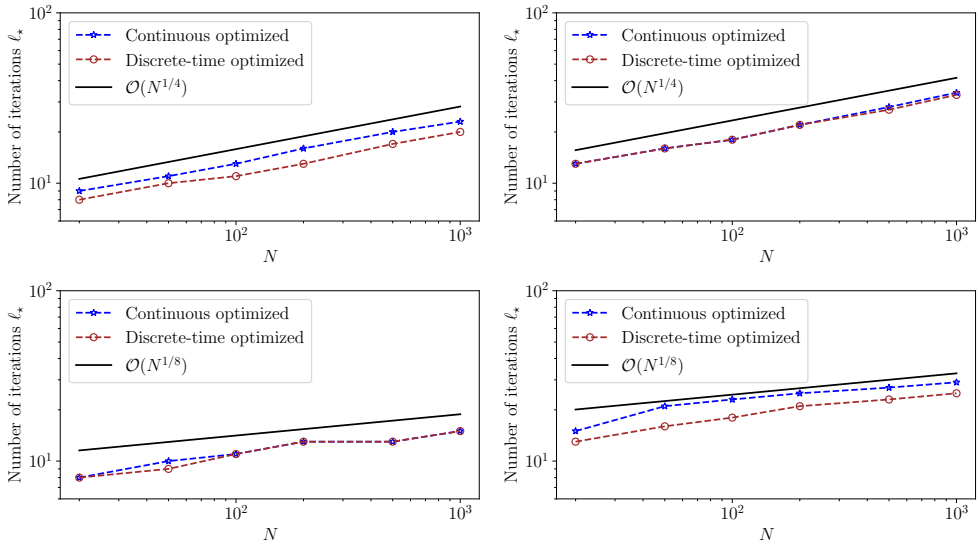

FIG. 9. *Asymptotic behavior : number of iterations $\ell_\star$ to obtain a relative L^∞-error smaller than 10^{-3} (left figures) and 10^{-6} (right figures), as a function of N, with $\Delta x = 5 \times 10^{-5}$, with continuous and discrete-time optimized parameters, in one-sided (top) and two-sided (bottom) cases.*

to reduce the relative L^∞-error by a factor 10^{-3} (left figures) and 10^{-6} (right figures),

as a function of N, on a log-log plot, in the one-sided case (top figures) and in the two-sided case (bottom figures). On top figures, the blue star curves are obtained with $\bar{\alpha}_C$, and the brown circle curves with $\bar{\alpha}_{D[\ell_A]}$, where $(\bar{\alpha}_{D[\ell_A]}, \ell_A)$ is obtained by Abacus 5.3 to reach 10^{-3} (top left) and 10^{-6} (top right); e.g. for $N = 200$, Abacus 5.3 gives $\ell_A = 23$ to reach 10^{-6}, then, choosing $\bar{\alpha} = \bar{\alpha}_{D[23]} (= \bar{\alpha}_{D[22]}$ from Definition (4.21)) in the actual simulation, one needs $\ell_\star = 22$ iterations to actually reach the relative accuracy 10^{-6}. We proceed in a similar way in the two-sided case (bottom figures). Using that $\Delta t = \frac{T}{N}$, the numerical results show the following asymptotic behaviors :

- $\ell_\star = \mathcal{O}(N^{\frac{1}{4}}) = \mathcal{O}(\Delta t^{-\frac{1}{4}})$ in the one-sided case, both for discrete-time and continuous optimized parameters (as predicted in [14] for the latter).
- $\ell_\star = \mathcal{O}(N^{\frac{1}{8}}) = \mathcal{O}(\Delta t^{-\frac{1}{8}})$ in the two-sided case, both for discrete-time and continuous optimized parameters, i.e. $\ell_\star$ is virtually independent of N (or Δt) in that case.

These results show that discrete-time and continuous optimized parameters give similar asymptotic behaviors versus N (or Δt), very little dependent on N for one-sided, and almost independent of N (or Δt) for two-sided parameters.

5.6. Comparison with $\bar{\boldsymbol{\alpha}}_M$. In this test, we take $N = 100$. Figure 10 shows the relative L^∞-errors as a function of OSWR iterations, obtained with $\bar{\alpha}_M$ and $\bar{\boldsymbol{\alpha}}_M$ defined in (4.18), compared to those obtained with continuous and discrete-time optimized parameters. Using Remark 4.10, we find $\bar{\alpha}_M = 1$ and $\bar{\boldsymbol{\alpha}}_M = (0.02, 1)$. We observe that, except for the very first iterations, the convergence with $\bar{\alpha}_M$ (left) or $\bar{\boldsymbol{\alpha}}_M$ (right) is much slower than with the other parameters.

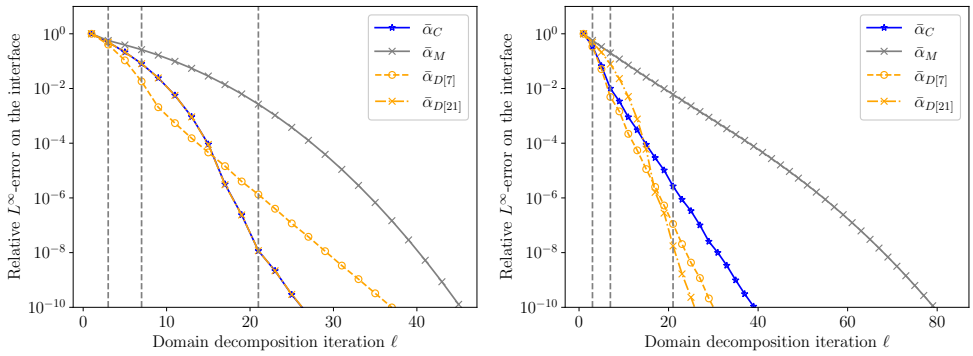

FIG. 10. *Comparison with parameters $\bar{\alpha}_M$ and $\bar{\boldsymbol{\alpha}}_M$: relative L^∞-errors computed with one-sided optimized parameters $\bar{\alpha}_C$, $\bar{\alpha}_M$, $\bar{\alpha}_{D[7]}$, $\bar{\alpha}_{D[21]}$ (left), and two-sided optimized parameters $\bar{\boldsymbol{\alpha}}_C$, $\bar{\boldsymbol{\alpha}}_M$, $\bar{\boldsymbol{\alpha}}_{D[7]}$, $\bar{\boldsymbol{\alpha}}_{D[21]}$ (right), for $\nu = 0.05$ and $N = 100$.*

6. Appendix.

6.1. Proof of Theorem 4.1.

Proof. Let us first consider the problem in Ω_1 in (4.4) : find U such that

$$\begin{array}{ll} LU & = 0 \quad \text{in } \Omega_1, \\ \lim\limits_{x \to -\infty} U(x) & \text{is bounded.} \end{array} \tag{6.1}$$

From Proposition 3.10, the matrix $C := \frac{1}{\sqrt{\nu \Delta t}} \sqrt{A}$ is lower triangular, invertible, with all its diagonal coefficients equal to $\frac{1}{\sqrt{\nu \Delta t}} > 0$.

Setting $Z \coloneqq \begin{pmatrix} U' \\ U \end{pmatrix}$, $\chi \coloneqq U'(x=0)$, $\Psi \coloneqq U(x=0)$, and $M \coloneqq \begin{pmatrix} 0 & C^2 \\ I & 0 \end{pmatrix}$, then problem (6.1) can be written into the equivalent first order differential system

$$\begin{array}{rcl} Z' & = & MZ \quad \text{in } (-\infty, 0) \\ Z(x=0) & = & (\chi, \Psi)^T \\ Z & & \text{is bounded in } (-\infty, 0) \end{array}$$

The solution of the above problem is given by

$$Z(x) = \mathrm{e}^{xM} \begin{pmatrix} \chi \\ \Psi \end{pmatrix}, \quad \forall x \in (-\infty, 0).$$

Using that $M^2 = \begin{pmatrix} C^2 & 0 \\ 0 & C^2 \end{pmatrix}$, by induction we have $M^{2k} = \begin{pmatrix} C^{2k} & 0 \\ 0 & C^{2k} \end{pmatrix}$ and $M^{2k+1} = \begin{pmatrix} 0 & C^{2k+2} \\ C^{2k} & 0 \end{pmatrix}$, $\forall k \in \mathbb{N}$, and thus

$$\begin{aligned} \mathrm{e}^{xM} &= \sum_{k=0}^{+\infty} \frac{x^{2k}}{2k!} M^{2k} + \sum_{k=0}^{+\infty} \frac{x^{2k+1}}{(2k+1)!} M^{2k+1} \\ &= \sum_{k=0}^{+\infty} \frac{x^{2k}}{2k!} \begin{pmatrix} C^{2k} & 0 \\ 0 & C^{2k} \end{pmatrix} + \sum_{k=0}^{+\infty} \frac{x^{2k+1}}{(2k+1)!} \begin{pmatrix} 0 & C^{2k+1} C \\ C^{2k+1} C^{-1} & 0 \end{pmatrix} \\ &= \begin{pmatrix} \operatorname{ch}(xC) & 0 \\ 0 & \operatorname{ch}(xC) \end{pmatrix} + \begin{pmatrix} 0 & \operatorname{sh}(xC)\, C \\ \operatorname{sh}(xC)\, C^{-1} & 0 \end{pmatrix} \\ &= \begin{pmatrix} \operatorname{ch}(xC) & \operatorname{sh}(xC)\, C \\ \operatorname{sh}(xC)\, C^{-1} & \operatorname{ch}(xC) \end{pmatrix}. \end{aligned}$$

Then we have, $\forall x \in (-\infty, 0)$,

$$\begin{pmatrix} U'(x) \\ U(x) \end{pmatrix} = \begin{pmatrix} \operatorname{ch}(xC) & \operatorname{sh}(xC)\, C \\ \operatorname{sh}(xC)\, C^{-1} & \operatorname{ch}(xC) \end{pmatrix} \begin{pmatrix} \chi \\ \Psi \end{pmatrix},$$

from which we obtain, $\forall x \in (-\infty, 0)$,

$$U(x) = \operatorname{sh}(xC)\, C^{-1} \chi + \operatorname{ch}(xC)\, \Psi.$$

The solutions of the system can therefore be written as follows

$$U(x) = \mathrm{e}^{xC} \beta^+ + \mathrm{e}^{-xC} \beta^-, \tag{6.2}$$

where $\beta^+ \in \mathbb{R}^N$ and $\beta^- \in \mathbb{R}^N$ will be determined using the boundary conditions.

More precisely, let us show that the condition U is bounded in $(-\infty, 0)$ implies that $\beta^- = 0_N$. We set

$$\mathcal{E}(x) \coloneqq \exp(-xC)\, \beta^-. \tag{6.3}$$

Since C is lower triangular, so are the sums and multiples of C. Coming back to the definition of the exponential of a matrix (with power series), we deduce that $\exp(-xC)$ is a lower triangular matrix whose diagonal is only composed of the exponential of $-\frac{x}{\sqrt{\nu \Delta t}}$. Thus, the first line of (6.3) gives $(\mathcal{E}(x))_1 = \mathrm{e}^{\frac{-x}{\sqrt{\nu \Delta t}}} (\beta^-)_1$, with $\frac{1}{\sqrt{\nu \Delta t}} > 0$. Since U (and thus $\mathcal{E}$) is bounded as x tends to $-\infty$, we deduce that

$(\beta^-)_1 = 0$. Then, the second line of (6.3) gives $(\beta^-)_2 = 0$, and by induction we obtain $\beta^- = 0_N$. Thus, the solutions of (6.1) are of the form $U(x) = \mathrm{e}^{xC}\beta^+$, with $\beta^+ \in \mathbb{R}^N$. The problem in Ω_2 is treated similarly to that in Ω_1, by using a change of variables, which end the proof of Theorem 4.1. ∎

REFERENCES

[1] E. Ahmed, C. Japhet, and M. Kern, *Spacetime domain decomposition for two-phase flow between different rock types*, Computer Methods in Applied Mechanics and Engineering, 371 (2020), p. 113294.

[2] S. Ali Hassan, C. Japhet, and M. Vohralík, *A posteriori stopping criteria for space-time domain decomposition for the heat equation in mixed formulations*, Electron. Trans. Numer. Anal., 49 (2018), pp. 151–181.

[3] P.-M. Berthe, C. Japhet, and P. Omnes, *Space–time domain decomposition with finite volumes for porous media applications*, in Domain Decomposition Methods in Science and Engineering XXI, J. Erhel, M. J. Gander, L. Halpern, G. Pichot, T. Sassi, and O. Widlund, eds., Cham, 2014, Springer International Publishing, pp. 567–575.

[4] E. Blayo, L. Halpern, and C. Japhet, *Optimized Schwarz waveform relaxation algorithms with nonconforming time discretization for coupling convection-diffusion problems with discontinuous coefficients*, in Domain Decomposition Methods in Science and Engineering XVI, O. B. Widlund and D. E. Keyes, eds., Berlin, Heidelberg, 2007, Springer Berlin Heidelberg, pp. 267–274.

[5] E. Blayo, A. Rousseau, and M. Tayachi, *Boundary conditions and Schwarz waveform relaxation method for linear viscous Shallow Water equations in hydrodynamics*, The SMAI journal of computational mathematics, 3 (2017), pp. 117–137.

[6] D. Q. Bui, C. Japhet, Y. Maday, and P. Omnes, *Coupling parareal with optimized Schwarz waveform relaxation for parabolic problems*, SIAM Journal on Numerical Analysis, 60 (2022), pp. 913–939.

[7] O. Ciobanu, L. Halpern, X. Juvigny, and J. Ryan, *Overlapping Domain Decomposition Applied to the Navier–Stokes Equations*, in Domain Decomposition Methods in Science and Engineering XXII, T. Dickopf, M. J. Gander, L. Halpern, R. Krause, and L. F. Pavarino, eds., Cham, 2016, Springer International Publishing, pp. 461–470.

[8] S. Clement, F. Lemarié, and E. Blayo, *Discrete analysis of Schwarz waveform relaxation for a diffusion reaction problem with discontinuous coefficients*, SMAI J. Comput. Math., 8 (2022), pp. 99–124.

[9] S. Descombes, V. Dolean, and M. J. Gander, *Schwarz waveform relaxation methods for systems of semi-linear reaction-diffusion equations*, in Domain Decomposition Methods in Science and Engineering XIX, Y. Huang, R. Kornhuber, O. Widlund, and J. Xu, eds., Berlin, Heidelberg, 2011, Springer Berlin Heidelberg, pp. 423–430.

[10] J. W. Eaton, D. Bateman, S. Hauberg, and R. Wehbring, *GNU Octave version 7.1.0 manual: a high-level interactive language for numerical computations*, 2022.

[11] M. J. Gander, *Overlapping Schwarz Waveform Relaxation for Parabolic Problems*, in Tenth International Conference on Domain Decomposition Methods. Contemporary Mathematics, J. Mandel, C. Farhat, and X.-C. Cai, eds., vol. 218, AMS, Boulder, CO, 1998.

[12] M. J. Gander, *Optimized Schwarz Methods*, SIAM J. Numerical Analysis, 44 (2006), pp. 699–731.

[13] M. J. Gander and L. Halpern, *Méthodes de relaxation d'ondes (SWR) pour l'équation de la chaleur en dimension 1. (Optimized Schwarz waveform relaxation (SWR) for the one-dimensional heat equation)*, C. R., Math., Acad. Sci. Paris, 336 (2003), pp. 519–524.

[14] ———, *Optimized Schwarz waveform relaxation methods for advection reaction diffusion problems*, SIAM J. Numer. Anal., 45 (2007), pp. 666–697.

[15] M. J. Gander, L. Halpern, and F. Nataf, *Optimal Schwarz waveform relaxation for the one dimensional wave equation*, SIAM J. Numer. Anal., 41 (2003), pp. 1643–1681.

[16] M. J. Gander, Y. Jiang, and B. Song, *A superlinear convergence estimate for the parareal Schwarz waveform relaxation algorithm*, SIAM Journal on Scientific Computing, 41 (2019), pp. A1148–A1169.

[17] M. J. Gander and V. Martin, *A detailed Fourier mode analysis of Schwarz waveform relaxation methods*. Contributed lecture at the 27th International Domain Decomposition Conference, DD27, Prague, Czech Republic, 2022.

[18] M. J. Gander and A. M. Stuart, *Space-time continuous analysis of waveform relaxation for the heat equation*, SIAM Journal on Scientific Computing, 19 (1998), pp. 2014–2031.

[19] E. Giladi and H. Keller, *Space-time domain decomposition for parabolic problems*, Numerische Mathematik, 93 (2002), pp. 279–313.
[20] G. H. Golub and C. F. Van Loan, *Matrix Computations*, Johns Hopkins University Press, 1996.
[21] R. Guetat, *Mthode de paralllisation en temps : application aux mthodes de dcomposition de domaine*, PhD thesis, UPMC Universit Paris 6 et Ecole polytechnique de Tunisie, 2011.
[22] F. Haeberlein, *Mthodes de dcomposition de domaine espace temps pour le transport ractif : Application au stockage gologique de CO2*, PhD thesis, Universit Paris 13, 2011.
[23] L. Halpern, C. Japhet, and J. Szeftel, *Optimized Schwarz waveform relaxation and discontinuous Galerkin time stepping for heterogeneous problems*, SIAM J. Numer. Anal., 50 (2012), pp. 2588–2611.
[24] R. D. Haynes and K. Mohammad, *Fully discrete Schwarz waveform relaxation on two bounded overlapping subdomains*, in Domain Decomposition Methods in Science and Engineering XXV, R. Haynes, S. MacLachlan, X.-C. Cai, L. Halpern, H. H. Kim, A. Klawonn, and O. Widlund, eds., Cham, 2020, Springer International Publishing, pp. 159–166.
[25] T.-T.-P. Hoang, J. Jaffré, C. Japhet, M. Kern, and J. E. Roberts, *Space-time domain decomposition methods for diffusion problems in mixed formulations*, SIAM J. Numer. Anal., 51 (2013), pp. 3532–3559.
[26] T.-T.-P. Hoang, Japhet, M. Kern, and J. E. Roberts, *Space-Time Domain Decomposition for Reduced Fracture Models in Mixed Formulation*, SIAM J. Numer. Anal., 54 (2016), pp. 288–316.
[27] C. Japhet and F. Nataf, *The best interface conditions for domain decomposition methods: absorbing boundary conditions*, in Absorbing Boundaries and Layers, Domain Decomposition Methods, Nova Sci. Publ., Huntington, NY, 2001, pp. 348–373.
[28] C. Japhet, F. Nataf, and F. Rogier, *The Optimized Order 2 method: Application to convectiondiffusion problems*, Future Generation Computer Systems, 18 (2001), pp. 17–30.
[29] J.-L. Lions and E. Magenes, *Non-homogeneous boundary value problems and applications. Vol. I*, Springer-Verlag, New York, 1972. Translated from the French by P. Kenneth, Die Grundlehren der mathematischen Wissenschaften, Band 181.
[30] ———, *Non-homogeneous boundary value problems and applications. Vol. II*, Springer-Verlag, New York, 1972. Translated from the French by P. Kenneth, Die Grundlehren der mathematischen Wissenschaften, Band 182.
[31] P.-L. Lions, *On the Schwarz alternating method. III: a variant for nonoverlapping subdomains*, in Third International Symposium on Domain Decomposition Methods for Partial Differential Equations, held in Houston, Texas, March 20-22, 1989, T. F. Chan, R. Glowinski, J. Périaux, and O. Widlund, eds., Philadelphia, PA, SIAM, 1990, pp. 202–223.
[32] V. Martin, *An optimized Schwarz waveform relaxation method for the unsteady convection diffusion equation in two dimensions*, Appl. Numer. Math., 52 (2005), pp. 401–428.
[33] ———, *Schwarz waveform relaxation algorithms for the linear viscous equatorial shallow water equations*, SIAM J. Scientific Computing, 31 (2009), pp. 3595–3625.
[34] D. Serre, *Les matrices - Théorie et pratique*, Dunod, 2001.
[35] S. Thery, *On the links between observed and theoretical convergence rates for Schwarz waveform relaxation algorithm for the time-dependent problems*, in 26th International Domain Decomposition Conference, Dec 2020, Hong Kong, China., 2020.
[36] S. Thery, C. Pelletier, F. Lemarié, and E. Blayo, *Analysis of Schwarz Waveform Relaxation for the Coupled Ekman Boundary Layer Problem with Continuously Variable Coefficients*, Numerical Algorithms, 89 (2022), pp. 1145–1181.
[37] C. W. Ueberhuber, *Numerical Computation 2*, Springer, 1995.
[38] S.-L. Wu, *Schwarz waveform relaxation algorithm for heat equations with distributed delay*, Thermal Science, 20 (2016), pp. 659–667.